Non-thermal Plasma Inactivation of *Bacillus Amyloliquefaciens* Spores

A Thesis Presented for the
Master of Science
Degree
The University of Tennessee, Knoxville

Yaohua Huang
August 2011

ACKNOWLEDGEMENTS

I am deeply indebted to my advisor professor Dr. Xiaofei P. Ye, whose help, stimulating suggestions and encouragement helped me in all the time of research and writing of this thesis. I would like to express my gratitude to my committee members Dr. Arnold Saxton and Dr. Mark Radosevich for their invaluable help and guidance throughout my studies and research.

My colleagues, Dr. Leming Cheng, Shirley Liu, Lu Chen, Dr. Guodong Wen, Dr. Quansheng Chen, Dr. Siqun Wang, Dr. John Dunlap and Margaret Taylor, from the Univeristy of Tennessee supported me in my research work. I want to thank them for all their help, support, interest and valuable hints. I appreciate undergraduate David Wang for his assistance in inactivation kinetic curve measurement.

Especially, I would like to give my special thanks to my family whose patient love enabled me to complete this work.

ABSTRACT

Bacterial spores have remarkable resistance to a variety of harsh conditions, causing spoilage in food industry and becoming the primary bacterial agent in biowarfare and bioterrorism. In this study, inactivation mechanisms of *Bacillus amyloliquefaciens* (BA) spores by non-thermal plasma (NTP) were investigated by using Fourier-transform infrared spectroscopy (FTIR) as a major tool to exam spores after NTP treatment. Chemometric techniques, such as multivariate classification models based on soft independent modeling of Class Analogy (SIMCA) and Principal Component Analysis (PCA), were employed to identify functional group changes in FTIR spectra. The IR absorbance bands correlated to dipicolinic acid (DPA) decreased after NTP treatment indicating that DPA released and then reacted with reactive species generated by NTP and it was confirmed by nuclear magnetic resonance (NMR). Also IR absorbance bands corresponding to protein structure changed. FTIR combined with UV-Vis spectroscopy was used to monitor spore germination. Large amount of DPA released in a short time when spores germinated at 50 ℃, showing that DPA released in response to heating. NTP treated spores could germinate with little DPA release due to sub-lethal effects induced by plasma. Also an empirical model based on Weibull distribution was established to describe the spore germination process showing that NTP treated spores exhibited abnormal germination pattern. Inactivation mechanisms of NTP with air as feed gas was compared with high-pressure, wet heat, chemical treatment using chlorine dioxide (CD) and NTP with argon as feed gas. The results showed that few chemical changes in spores after autoclave and high pressure treatments, though protein structure changed. CD and

NTP with air as feed gas inactivated spores by oxidation. DPA released after NTP with argon as feed gas treatment and it is possible that UV and charged particles accounts for the inactivation. This study provides in depth insight into the inactivation mechanism of NTP and information for optimizing NTP process.

TABLE OF CONTENTS

Page

CHAPTER I 1
Introduction and Objective 1
1.1 Bacterial spore 1
1.2 Significances of non-thermal plasma 2
1.3 A rapid tool to characterize spores: Attenuated total reflection Fourier-transform infrared spectroscopy (ATR-FTIR) 3
Objective 5
CHAPTER II 7
Literature Review 7
2.1 Spore structure 7
2.2 Spore formation 9
2.3 Spore germination 10
2.4 Non-thermal plasma inactivation of spores 11
2.4.1 Non-thermal plasma generation at atmospheric pressure through gas discharges 11
2.4.2 Calculation of energy consumption of non-thermal plasma by Lissajous figure 13
2.4.3 Kinetics of the bacterial inactivation process 14
2.4.4 Possible inactivation mechanism 17
2.4.5 Sub-lethal study: spore germination after plasma treatment 21
2.5 Investigation of biochemical changes in bacterial spores by Fourier transform infrared spectroscopy 21
2.6 Real time monitoring of spore germination by attenuated total reflection Fourier-transform infrared spectroscopy 23
CHAPTER III 24
Inactivation Mechanisms of *Bacillus amyloliquefaciens* spores by Non-thermal Plasma 24
Abstract 24
3.1 Introduction 25
3.2 Materials & Methods 26
3.2.1 Spore preparation 26
3.2.2 Plasma generation and energy consumption measurement 27
3.2.3 Plasma inactivation kinetics 28
3.2.4 Spore morphology observation 28
3.2.5 Spore surface analysis by atomic force microscopy 29
3.2.6 Attenuated total reflection Fourier-transform infrared spectroscopy analysis of spore after NTP treatment 29
3.2.7 Nuclear magnetic resonance analysis of DPA 30

3.3 Results and Discussion 31
3.3.1 Kinetics of plasma inactivation of BA spores 31
3.3.2 Energy consumption in NTP treatment 36
3.3.3 Morphology observation 37
3.3.4 Fourier transform infrared spectroscopy analysis 40
3.3.5 NMR analysis of DPA 45
3.4 Conclusion 45
CHAPTER IV 47
Characterization and Modeling of Bacterial Spore Germination Using FTIR and UV-Vis Spectroscopy 47
Abstract 47
4.1 Introduction 47
4.2 Materials & Methods 49
4.2.1 Spore preparation 49
4.2.2 Non-thermal plasma inactivation of spores 49
4.2.3 ATR-FTIR real time monitoring of spore germination 50
4.2.4 Monitoring spore germination by UV-Vis spectroscopy 50
4.2.5 Modeling of spores germination 51
4.2.6 Validation of model performance 52
4.3 Results and discussion 52
4.3.1 ATR-FTIR and UV-Vis spectroscopy analysis during spore germination at different temperatures 52
4.3.2 Germination of spores after sub-lethal NTP treatment 57
4.3.3 Modeling of spore germination 59
4.4 Conclusion 62
CHAPTER V 64
Comparison of Mechanisms of Inactivation of *Bacillus amyloliquefaciens* Spores Using FTIR 64
Abstract 64
5.1 Introduction 65
5.2 Materials & Methods 66
5.2.1 Spore preparation 66
5.2.2 Morphology study by Scanning Electron Microscope 66
5.2.3 Morphology study by Transmission Electron Microscopy 67
5.2.4 Fourier transform infrared spectroscopy analysis 68
5.3 Results and Discussion 69
5.3.1 Morphology study by scanning electron microscope 69
5.3.2 Observation by transmission electron microscopy 71
5.3.3 Fourier transform infrared spectroscopy analysis 72
5.5 Conclusion 81
OVERALL SUMMARY AND PERSPECTIVE 83
LIST OF REFERENCES 86
Vita 94

LIST OF TABLES

Table Page

Table 3-1 Kinetics data of plasma inactivation..... 32
Table 3-2 Assignment of Bands in the FT-IR Spectra of Bacterial..... 40

Table 4-1The Weibull model parameters rate index (α) and behavior index (β) at different temperatures..... 60
Table 4-2 Empirical model accuracy (A_f) and bias factors (B_f) for the spore germination in different temperatures..... 60

LIST OF FIGURES

Figure Page

Figure 1- 1 Schematic diagram of ATR-FTIR: (A) multiple reflection ATR system; (B) single reflection ATR system..... 4
Figure 2- 1 Cross section of a spore 7
Figure 2- 2 Structure of (A) dipicolinic acid (DPA) and (B) calcium dipicolinate (Ca-DPA) 8
Figure 2- 3 Common DBD configuration with one or two dielectric barriers [36]..... 12
Figure 2- 4 Kinetics of the inactivation process. (a) Single-slope survival curve; (b) Bi-slope survival curve; and (c) Multi-slope survival curve [52]..... 16
Figure 2- 5 Basic reaction sequence for lipid (L) peroxidation by free radicals [54]..... 18
Figure 3- 1 Schematic diagram of plasma generation by dielectric barrier discharges 27
Figure 3- 2 Survival plot of spores after NTP treatment for different times 33
Figure 3- 3 Topography images of spore surface: (A) control; (B) plasma treated for 1 min 35
Figure 3- 4 Lissajous figure of discharge 36
Figure 3- 5 SEM imaging: (A) Dried control, (B) Dried spores plasma treated for 1 min; (C) Dried spores plasma treated for 3 min; (D) Dried spores plasma treated for 5 min; (E) Wet spores plasma treated for 1 min; (F) Wet spores plasma treated for 3 min. 39
Figure 3- 6 ATR-FTIR spectrum of spores: (A) control; (B) 1 min plasma treated; (C) 3 min plasma treated; (D) 5 min plasma treated 41
Figure 3- 7 Soft independent modeling of class analogy class projections of spores under different treatment time..... 41
Figure 3- 8 Discriminating power in classification of treated spores with control. Prominent bands and their relative importance in discriminating control and (A) 1 min; (B) 3 min; (C) 5 min plasma treated spores..... 43
Figure 3- 9 ^{1}H NMR spectrum of spore extraction: (A) control; (B) 1 min; (C) 3 min; (D) 5 min; (E) standard DPA. Numbers were normalized integrals of DPA peaks..... 44
Figure 4- 1 Three-dimensional spectrums of germinating spores (A) control at 23 ℃; (B) plasma treated spores at 23 ℃..... 53
Figure 4- 2 Absorbance of the Ca-DPA specific IR band at 1570 cm^{-1} as a function of time in spore germination: (A) 23 ℃; (B) 30 ℃; (C) 40 ℃; (D) 50 ℃; (E) 23 ℃, plasma treated. 54
Figure 4- 3 Germination curve of spores germinated in (A) 23 ℃, (B) 30 ℃, (C) 40 ℃, (D) 50 ℃ as measured by $OD_{600.}$ 55
Figure 4- 4 The fraction of germinated spores versus the intensities of the Ca-DPA specific band at 1570 cm^{-1} 56
Figure 4- 5 Absorbance at significant wavelengths at different time: (A) control; (B) plasma treated spores 58
Figure 4- 6 Scatter plot of fraction of germinated spores (S) and Weibull model predicted line of S over time..... 61
Figure 5- 1 SEM image of dried BA samples: (A) control; (B) chemical (CD) treated; (C) autoclaved; (D) high-pressure treated; (E) non-thermal plasma(NTP) using air as feed gas treated; (F) NTP using argon as feed gas treated..... 69

Figure 5- 2Transmission electron microscopic images of the fixed BA samples: (A) control; (B) chemical treated (CD); (C) autoclaved; (D) high pressure treated; and (E) non-thermal plasma treated with 20,000 magnification (left column) and 10,000 magnification (right) 71
Figure 5- 3 FT-IR spectra of control spores and spores after (A) autoclave, (B) pressure, (C) chemical treated (CD), (D) control, (E) NTP with air as feed gas, (F) NTP with argon as feed gas treatments. 73
Figure 5- 4Score plot of all samples in PC1, PC2 and PC3: Control (C), Autoclave (A), chlorine dioxide (CD), High pressure (P), Non-thermal plasma (NTP). 74
Figure 5- 5 SIMCA analysis of control and spores after Chemical (CD) and NTP (air or argon as feed gas) treatments 76
Figure 5- 6 Survival curve of (A) NTP (air), (B) NTP (argon) inactivation process 78
Figure 5- 7 Principal component analysis of control spores and spores after autoclave treatment 80
Figure 5- 8 Principal component analysis of control spores and spores after high pressure treatment 81

CHAPTER I
Introduction and Objective

1.1 Bacterial spore

Bacteria spore is a dormant or inactive cell type produced by gram-positive bacteria species in response to adverse conditions, such as starvation, extreme temperatures, ionizing radiation, mechanical force, chemical solvents, detergents, hydrolytic enzymes, desiccation, pH extremes and antibiotics [1]. Spore germinates when it is in the presence of appropriate environment: adequate amino acids, sugars, water, and a favorable pH and temperature.

The longevity of spores in the environment is an important factor in the anthrax epidemiology and causes the food safety issue [2]. Terrorism is a serious concern around the world and we are at risk from terrorist attack, especially biological attack [3, 4]. A *Bacillus* spore, anthrax, has become the primary bacterial agent in biowarfare and bioterrorism. Terrorists can easily store spores and rapidly produce bio-weapons by anthrax. Its fatal nature and strong viability in the environment after bioattack makes it more minatory [2].

Spoilage caused by spores often results in large economic losses and has become a primary concern in the food industry. For example, the gram-positive, rod-shaped, spore-forming acidophilic thermophile *Alicyclobacillus* has been recognized as a significant spoilage organism in beverages [5] and *Clostridium perfringens* is an anaerobic endospore forming Gram-positive bacteria and a significant cause of histotoxic and gastrointestinal (GI) diseases in humans and animals [6]. The spore-forming nature of

these organisms enables them to exhibit high resistance to harsh conditions, leading to spoilage in food products and even food poisoning outbreaks.

Above all, efficient spore inactivation approaches are demanded to counter terrorism and meet consumer expectations for increased food safety, extended shelf life and improved food quality.

Spores formed by anaerobes of the genus *Clostridium* and facultative aerobes of the genus *Bacillus* are omnipresent in the environment and well-known as model spores [1]. In this study, *Bacillus amyloliquefaciens* (BA) spore was chosen as model spore because it is innocuous and reproducible with consistent quality by a standard protocol. Also it is closely related to *Bacillus anthracis* that were deployed in the bio-terrorist attacks in the United States [7] and it is a surrogate to *Clostridium perfringens* which is found in meat and can cause food-borne diseases [8].

1.2 Significances of non-thermal plasma

Microorganism control and decontamination are crucial to food and pharmaceutical industrial safety assessments. However, many materials used in food and pharmaceutical packaging are not compatible with standard heat sterilization treatments. Most polymers used as materials in our daily life are poorly resistant to heating so that oven or autoclave sterilization processes are generally infeasible [9]. After thermal sterilization, these polymers can be decomposed into carcinogens, such as dioxins. Above all, non-thermal methods are demanded in sterilization of heat-sensitive materials and food.

Non-thermal plasma is a newly developing method. It is more cost-efficient and environmentally friendly compared with traditional autoclave and chemical treatments. It is regarded as a potential alternative to conventional sterilization methods used in food processing. Plasma is the defined as the fourth state of matter, following by order of increasing energy, the solid state, the liquid state and the gaseous state. The most commonly used plasma for sterilization purpose is known as cold plasmas or non-thermal plasmas (NTP) with reference to their gas temperature [10]. They are neutral ionized gases constituted of not only ions and electrons, but also uncharged particles including photons, atoms, reactive species, and excited or non-excited molecules. Non-thermal plasma can inactivate spores up to 10 $\log_{10}$CFU (Colony Forming Unit) in a short time (less than 10 min) and is economically viable due to relatively low installation costs and energy consumption [9].

1.3 A rapid tool to characterize spores: Attenuated total reflection Fourier-transform infrared spectroscopy (ATR-FTIR)

Mid-Infrared (IR) spectroscopy is a reliable method to characterize, identify and quantify many substances [11]. IR spectroscopy can obtain spectra from a very wide range of solids, liquids and gases but sample preparation is required in order to obtain a good quality spectrum.

The technique of Attenuated Total Reflectance (ATR) simplifies the sample preparation process and improves spectral reproducibility. It has been a revolution for solid and liquid sample analyses in recent years.

An infrared beam is directed onto an optically dense crystal with a high refractive index at a certain angle and then extends beyond the surface of the crystal and protrudes only a few microns (0.5 μm - 5 μm) into the sample held in contact with the crystal. In regions of the infrared spectrum where the sample absorbs energy, the evanescent wave will be attenuated or altered [11]. Since the sample has lower refractive index than the crystal, the infrared beam exhibits total reflection then exits the opposite end of the crystal and is passed to the detector in the IR spectrometer [11]. The detector measures the changes in the totally internally reflected infrared beam and generates an infrared spectrum (Figure 1-1).

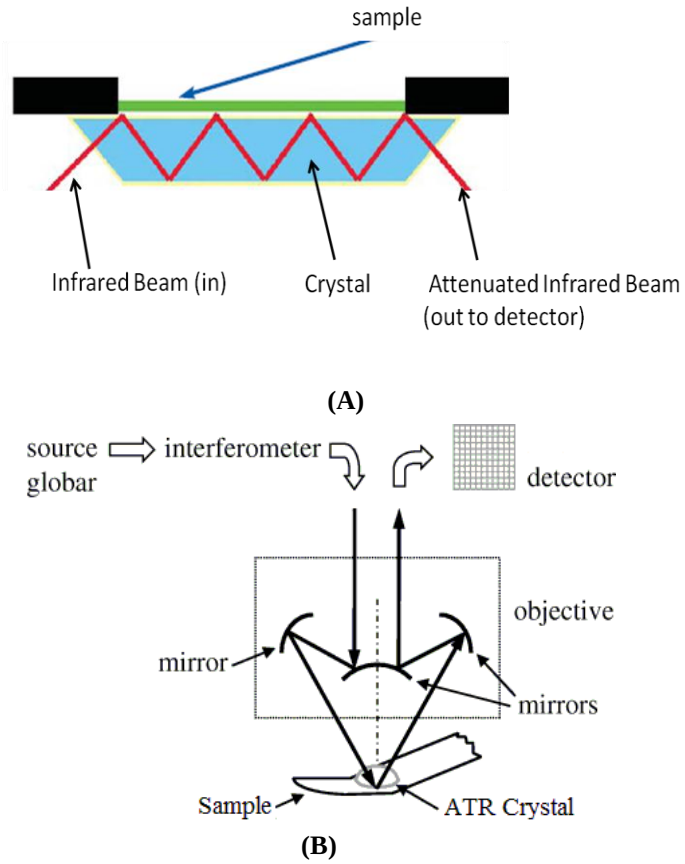


Figure 1- 1 Schematic diagram of ATR-FTIR: (A) multiple reflection ATR system; (B) single reflection ATR system

Attenuated total reflection Fourier-transform infrared spectroscopy (ATR-FTIR) is an easy and sensitive technique providing structural and chemical information at the molecular level. Some cellular components of bacteria can be identified by infrared spectroscopy [12], and constituents such as lipids, dipicolinic acid (DPA) and intracellular materials have been detected with this method [13].

Therefore, it is a powerful tool for obtaining useful chemical information of spores before and after non-thermal plasma treatment without any complicated sample preparation.

In this study, the single reflection ATR system detected all cellular components and constituents because spores were pressed and tightly in contact with the ATR crystal and the penetration depth was larger than the spore diameter; while the signal of multiple reflections ATR system accounted for chemicals released by spores because spores were in the liquid ST1 medium and did not have a good contact with ATR crystal.

Objective

The objective of this study was to provide insights into non-thermal plasma (NTP) inactivation of bacterial spores using ATR-FTIR as a major tool to probe the biochemical and structural changes of bacterial spores, in order to better manipulate and optimize the parameters for the NTP processing.

Specifically, the following tasks were conducted:

1. To study inactivation mechanisms of *Bacillus amyloliquefaciens* spores by non-thermal plasma using FTIR;

2. To characterize and model bacterial spore germination at different temperatures and after NTP treatment using FTIR and UV-Vis spectroscopy;
3. To compare mechanisms of inactivation of *Bacillus amyloliquefaciens* spores by high-pressure, wet heat, chlorine dioxide and non-thermal plasma (NTP) with air or argon as feed gas.

CHAPTER II
Literature Review

2.1 Spore structure

The unique structure of bacterial spores confers them the remarkable resistance to harsh environment. The spore is composed of following five main parts as shown in Figure 2-1: exosporium, coats, cortex, inner membrane and core [14, 15]. Spore resistance to enzymes, mechanical disruption and some chemicals such as hydrogen peroxide is a function of spore coats; while the peptidoglycan cortex protects spore from organic solvents and binding of spore DNA by small acid soluble spore proteins in the spore core accounts for the protection of spore DNA from UV radiation and free radical damage [16]. In the following paragraph, each of the spore components is demonstrated with its respective role in dormancy, resistance and germination.

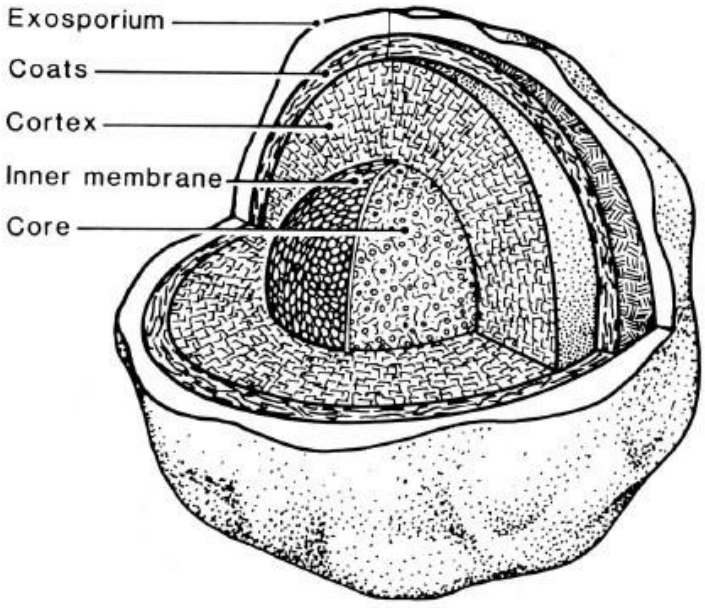


Figure 2- 1 Cross section of a spore [1]

The core contains the spore cytoplasm and cellular components such as cytoplasmatic proteins, ribosomes and DNA [1]. The water content of spore core is much lower (28 to 50% of wet weight) than the water content of the cortex, coat, and exosporium regions which is similar to that in vegetative cells (75 to 80% of wet weight) [17]. The dehydrated state is one of the most important features of spores that contributed to the remarkable resistance to adverse environment [1]. High levels of divalent cations, especially Ca^{2+}, are in the spore core and it is associated with resistance to wet-heat and oxidizing agents [17]. Besides, high concentration of divalent cations also results in low water content and it may contribute to wet heat resistance [17]. Many divalent cations (for example, calcium) are chelated with dipicolinic acid (DPA) and its structure is shown in Figure 2-2. DPA is also associated with dehydrated state of spore [18], wet heat [18] and H_2O_2 resistance [17]. Spore DNA forms a complex with a particular kind of proteins, termed small acid soluble proteins (SASP). SASP straightens and stiffens the DNA and decreases DNA's reactivity with a variety of chemicals so that protects the DNA against many kinds of damages [1, 17, 19].

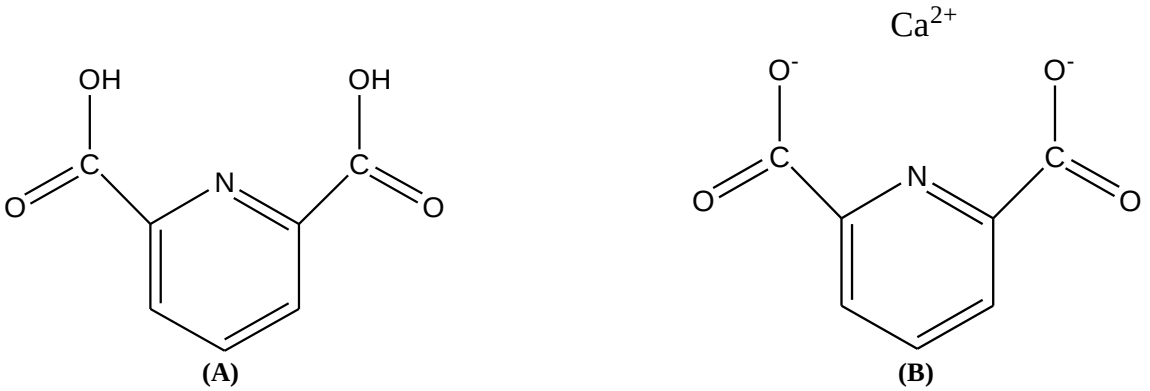


Figure 2- 2 Structure of (A) dipicolinic acid (DPA) and (B) calcium dipicolinate (Ca-DPA)

The inner membrane surrounds the spore core in a compressed state with lipids immobile. It is an important structure for spore resistance and germination because it serves as the main permeability barrier of spores and spore germination receptors located on it [1].

The cortex is a thick cell wall around the inner membrane that is composed of specifically modified peptidoglycan [1]. It plays an important role for the maintenance of spore core dehydration [20].

The germ cell wall is the inner part of the cortex that lacks the specific modifications of peptidoglycan.

The spore coats are dynamic protein structures generally consisting of three distinct layers that built around the cortex [1]. The spore coats protect the cortex peptidoglycan from enzymatic degradation [21]. They are involved in resistance to environmental UV radiation [1, 16, 17] and a variety of chemicals including oxidative agents [1, 17]. There is a lytic enzyme in spore coats that helps degrade the cortex during germination [22] and other coat proteins facilitating the passage of specific germinant molecules through the coats during germination [1, 23].

The exosporium is a loose, membrane-like structure in some species outside the spore coats and is important for spore hydrophobicity and adherence properties [24].

2.2 Spore formation

Spore formation is initialized when nutrients are insufficient or conditions become adverse. The DNA condenses and realigns itself in the center of the cell [25]. Next, the DNA divides into two complete copies and the vegetative cell undergoes an asymmetric

division that cell membrane invaginates to form the smaller developing fore-spore and the remaining vegetative cell formed a larger mother cell [26]. The mother cell membrane continues to grow and engulfs the fore-spore. The fore-spore is now surrounded by two membrane layers [27]. Then, peptidoglycan is laid down between the two membranes of the developing spore to form the cortex [25]. Dipicolinic acid (DPA) is formed inside the developing spore and calcium enters from the outside [28]. As calcium enters the spore, water is removed. A protein coat forms exterior to the cortex and the spore becomes mature. Some spores form an additional layer, as mentioned above, called exosporium. A mature spore is resistant to harsh conditions. Finally, the mother cell will be destroyed by lytic enzymes in a process of programmed cell death and the mature spore is released [1].

2.3 Spore germination

Spore germination is the process that a dormant spore develops into an active metabolizing vegetative cell and it involves the process of activation triggering of germination, initiation of germination and finally, outgrowth [29].

Germination can be activated by a variety of chemical and physical agents such as heat, hydrostatic pressure etc., but little are known about the mechanism of activation [1]. However, no change is detected either in the spore structure or composition during activation [30].

Activated spores will germinate when they are in conditions suitable for growth. Germinant receptors are specific proteins located in the plasma membrane [31] and they recognize some specific compounds, such as amino acids, sugars and ribosides [1], called

germinant. The germinant binds to the germinant receptors as a signal of right germination condition and triggers the germination process. Two types of chemicals, nutrient and non-nutrient types are known to initiate the triggering process [23, 32]. L-alanine is one of the effective germinant but the exact mechanism of activation is not yet clearly known.

In the beginning of germination process, cation H^+ and Zn^{2+} probably release from the spore core, followed by Ca-DPA release; then water replaces DPA and the core hydration increases while spore resistance to adverse environments decreases; then peptidoglycan of spore cortex hydrolyzed and further water uptake makes spore core swelled [32]. With the core hydration, protein mobility in the core returns and enables enzyme actions [32]. The spore metabolism is initialized by enzyme actions and followed by macromolecular synthesis. Finally germinated spore is converted into a growing cell and this process termed outgrowth [32].

2.4 Non-thermal plasma inactivation of spores

2.4.1 Non-thermal plasma generation at atmospheric pressure through gas discharges

The non-thermal plasma (at atmospheric pressure) does not require specific discharge gas and vacuum to achieve a lower pressure. Due to their design simplicity and low operating cost, this form of the discharge plays an important role in industry. In these plasmas, free electrons are accelerated by the electric field and collide with the background atoms and molecules, thereby releasing more electrons and causing enhanced level of dissociation, excitation and ionization, what is known as an electron

avalanche[33, 34]. The significant characteristic is that the operating gas temperature will not increase sharply during these reactions. The non-thermal feature of these plasmas makes it possible to treat heat-sensitive materials including food packages and biological tissues.

The non-thermal plasma can be generated by the dielectric barrier discharge (DBD), which is also known as silent discharge.

DBD is a special type of AC or RF discharge. It operates at 0.1-10 bar. DBD was originally developed for the generation of ozone from air or oxygen in 1857 and now is widely used for water treatment [35]. The gas discharge is generated between two electrodes, separated by one or more dielectric barriers and a gas filled gap (Figure 2-3), which inhibit the glow-to-arc transition.

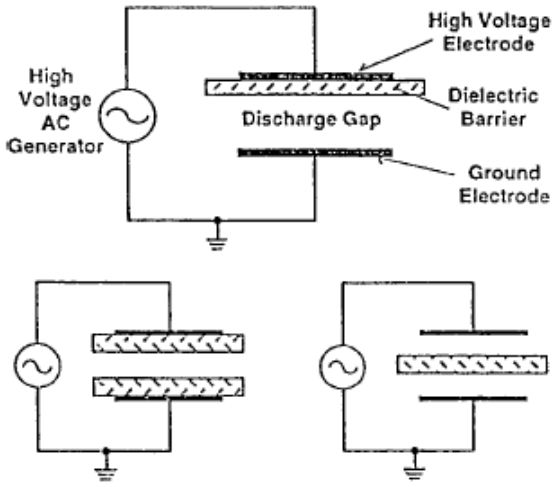


Figure 2- 3 Common DBD configuration with one or two dielectric barriers [36]

Different modes of discharge have been observed, from filamentary to completely diffuse barrier discharges. In most DBD configurations, the gas-filled gap is small (typically a few millimeters) and a voltage of 1-100kV with frequencies of 50 Hz- 1 MHz is necessary to sustain these discharges [37]. The streamer breakdown mechanism leads to formation of miniature filamentary discharges (diameter~0.1mm) called microdischarges. Most industrial applications of DBDs operate in this filamentary mode [38].

2.4.2 Calculation of energy consumption of non-thermal plasma by Lissajous figure

The typical way to calculate power is to measure the voltage and current, then power

$$P = \frac{1}{T}\int_0^T U(t)I(t)dt \qquad \text{Equation 1}$$

However, it is hard to calculate the power consumed in the dielectric-barrier discharge because the extremely short current pulses caused by individual microdischarges are difficult to measure with a current probe and the sensitivity of the current probes is not high enough to measure in a low power experiment [39]. Also the power should exclude the heat generated by the circuit and be only generated by plasma. A voltage-charge Lissajous figure can avoid these problems by measuring on a capacitor. Substitution of I(t)=dQ(t)/dt leads to:

$$P = \frac{1}{T}\oint U(Q)dQ = C_M f \oint U(U_{c)}dU_c \qquad \text{Equation 2}$$

where f is the frequency, Cm is capacitance and Uc is its corresponding voltage which is proportional to the charge. The integral has to be extended over one period T of the applied voltage [39]. The area of the figure display on the oscilloscope is equivalent to

the energy dissipated during one period.

2.4.3 Kinetics of the bacterial inactivation process

As a method of characterizing the inactivation efficiency and mechanisms by plasmas, survival curves are plots of the logarithm of the number of still living microorganisms (Colony Forming Unit, CFU) versus treatment time. The kinetics parameters for spore inactivation are estimated by the relationship between the count of survivors and time:

$$\log\left[\frac{N(t)}{N_0}\right] = -k \times t \qquad \text{Equation 3}$$

where N_0 is the initial spore count, N is the spore count after exposure to the plasma treatment for a specific time (t) and k is the 'death rate' constant [40].

'D' value (Decimal value), which is borrowed from studies on heat sterilization, is widely used in the studies of sterilization by plasma. The D-value is the time required for the original concentration of microorganisms to be reduced by 90%, in other words, the time for one log10 reduction. It is given by:

$$\log\left[\frac{N_s}{N_0}\right] = -\frac{t}{D} \qquad \text{Equation 4}$$

where t is the time to destroy 90% of the initial population, N_0 is the initial concentration and N_s is the surviving population [40].

So far, single-slope, bi-slope and multi-slope survival curves were reported on the germicidal effects of non-thermal, atmospheric pressure plasmas. It depends on several factors: the type of microorganism, the type of medium the cells are grown on, the

number of cell layers in the sample, the type of exposure, “direct exposure” or “remote exposure”, contribution of UV or not, operating gas mixture, etc.[40].

The different shapes of survival curves indicate that the inactivation process is complex. And the inactivation kinetics can provide insight into the microorganism inactivation mechanisms by plasma. Single-slope survival curves (Figure 2-4A) are reported in some cases [41-43]. It is the same as the conventional sterilizers such as the autoclave where the survival curve is composed of a single straight line.

Boudam et al.[44] concluded that inactivation by plasma exposure usually yields survival curves with two linear segments, but they did not give any evident to support it. In the reported two-slope survival curves (Figure 2-4B) by Kelly-Wintenberg et al.[45] and Laroussi et al.[46], the slope of the second line is steeper than the first line, which means the D-value of the second line (D_2) is smaller than the first line (D_1). Kelly-Wintenberg et al. [45] explained that during the first phase, the active species generated by the plasma alter the structure of the cell membrane and as the concentration reaches the lethal level, it will trigger the second phase resulting in the rapid lysis of the cells. It explains the short D_2 value. In later research, Kelly-Wintenberg et al. claimed that D_1 was varied according to the microorganism tested while D_2 depended on the type of medium supporting the microorganism [47].

Multi-slope survival curves (Figure 2-4C) were also observed [46, 48, 49]. The exact explanation for this type of curve is under debate. Moisan et al. [10] proposed an explanation that UV-induced photodesorption happened on the first layer of the stacked spores in the first phase, then followed by etching through active species adsorption in the second phase with slow kinetics. Finally, after the adsorption is saturated, the UV hits

the genetic material of the living spores. However, this explanation does not fit into the atmospheric-pressure non-thermal plasmas because the germicidal UV (200–290 nm) is not presented with sufficient intensity to inactivate spores [41, 43, 50].

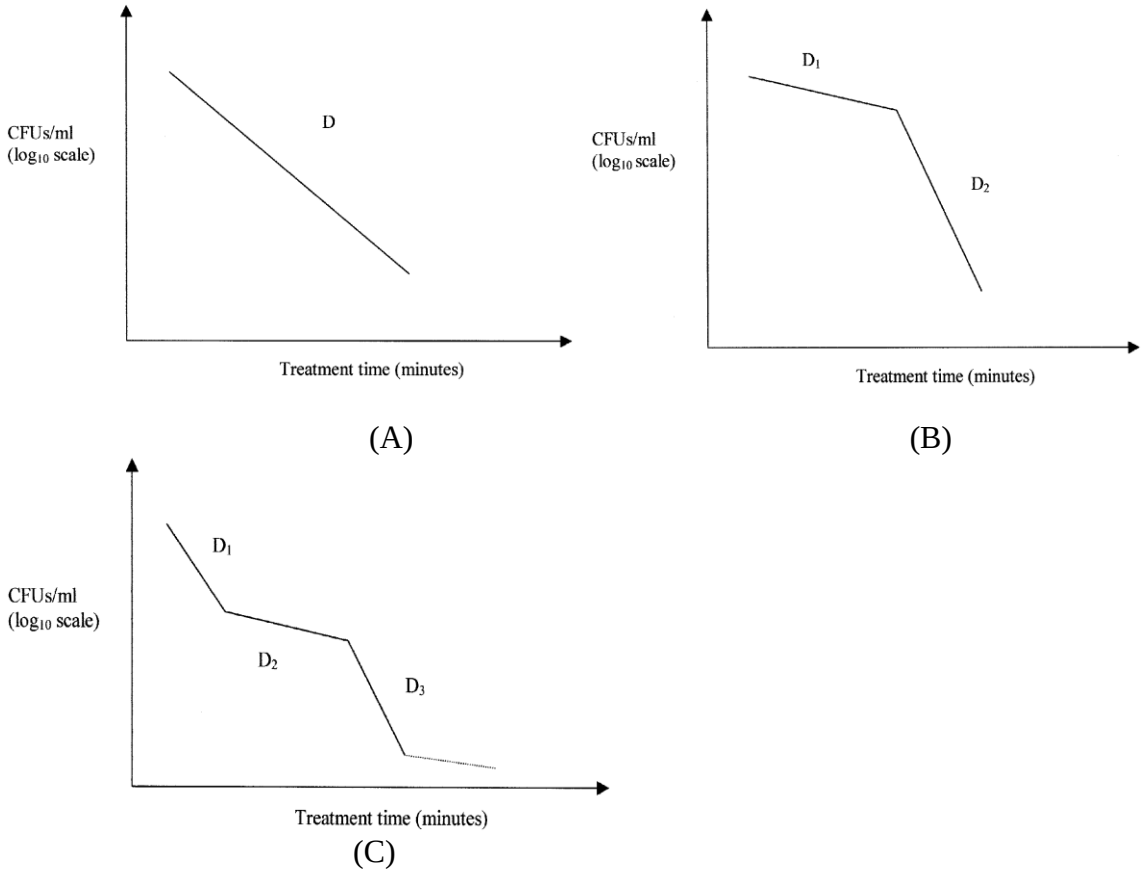


Figure 2- 4 Kinetics of the inactivation process. (a) Single-slope survival curve; (b) Bi-slope survival curve; and (c) Multi-slope survival curve [51].

2.4.4 Possible inactivation mechanism

2.4.4.1 UV irradiation

UV radiation is well known for its bactericidal properties. The energy in the photons of UV lights is absorbed by the genetic materials at certain wavelengths. Only when the UV spectrum is in the region 220-280 nm and meets the minimum dose of lesion to the DNA strands, will it have lethal damage to the microorganism by forming pyrimidine dimers in DNA, so that the bacteria cannot replicate properly [52]. There are three types of pyrimidine dimers formed: thymine-thymine (T◊T), thymine-cytosine (T◊C), and cytosine-cytosine (C◊C) [53]. The DNA base composition of the irradiated bacteria decides the type formed during UV irradiation [54]. Purines also absorb UV photons, however, due to the higher quantum yield required to synthesize dimers [55], the pyrimidine dimers are the dominating photoproducts.

In the low-pressure plasma (operated in 0.5 – 150 Pa), UV irradiation is considered to be the most important inactivation agent, while in the atmospheric pressure plasma using air (approximately 20% O_2 and 80% N_2) as discharging gas, the effects of UV irradiation can be neglected. Laroussi and Leipold [56] reported that there is no significant UV emission below 285 nm. Boudam [44] agreed with their conclusion in his review paper. Basically, the wavelength of UV emitted is not in the valid range of inactivation. Gaunt [53] claimed that UV emitted is reabsorbed (author did not mention reabsorbed by what) so that the lethal doses are not delivered.

2.4.4.2 Reactive species

In atmospheric pressure non-thermal plasma discharges, reactive species play an important role in plasma inactivation of spores. Reactive species are generated by electron collision. Compared to the low-pressure plasma, the atmospheric pressure discharge is dominated by reactive neutral species such as oxygen atoms, singlet oxygen (the common name used for the diamagnetic form of O_2) and ozone rather than ions [57, 58]. In gas discharges at atmospheric pressure in air, the main reactive species are ozone (O_3), atomic oxygen (O or O^-), superoxide (O_2^-), peroxide (O_2^{2-} or H_2O_2), hydroxyl radicals (OH●), nitric oxide (NO), nitrogen dioxide (NO_2).

Reactive species can cause damages in DNA, proteins, and lipids [59]. Cell membranes have lipid bilayers structure. Polyunsaturated fatty acid, an important component of lipid bilayers, is susceptible to the attack by radicals formed during oxidative stress, such as hydroperoxyl radicals (HOO●), superoxide radicals, singlet oxygen, and ozone [60]. They initiate lipid peroxidation and start a destructive chain reaction (Figure 2-5). Ozone can accelerate the chain reaction by oxidation and leads to a reduction of membrane fluidity [53].

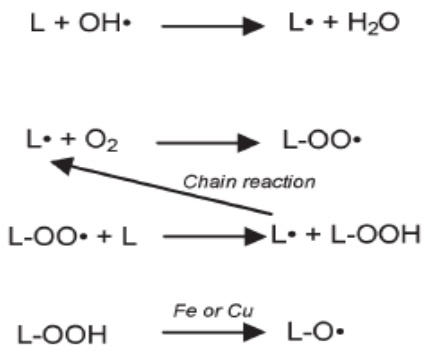


Figure 2- 5 Basic reaction sequence for lipid (L) peroxidation by free radicals [53].

The products of the chain reaction are shorter than the initial unsaturated fatty acids [60]. So the ability of unsaturated fatty acids to rotate within the membrane is altered [61] and the function of the membrane lipids is compromised. Disordered transportation of ions and polar compounds will lead to an osmotic imbalance, even cell lysis. Also lipid peroxidation generates aldehydes. They are very reactive and can damage proteins [62]. Compared with reactive species generated by plasma, aldehydes are more stable and can travel long distance to attack targets [53].

As for proteins, the reactive species react with the amino acid side chains and cause protein structure changes [59, 63, 64]. Ozone, in particular, can react with dienes, amines and thiols [60] and cross-link tyrosine residues by oxidizing the –OH groups. Proteins are inactivated without correct structure dimensions, which leads to malfunction in every aspect, especially metabolism of the cell and eventually damages the cell. Outer spore coat and inner spore coat of spores make them resistive to harsh conditions. However, these coats are composed of proteins and can be destructed by reactive species generated by plasma [40]. Besides, the accumulation of damaged proteins can otherwise compromise cell metabolism [59]. It is reported that the oxidized proteins cannot be degraded due to the inhibition of protease by heavily oxidized proteins [65, 66].

DNA can be damaged, with both bases and sugar moieties reacting with the reactive species. Besides, the intermediate radicals formed during lipid peroxidation are also reactive to DNA [60]. As mentioned before, aldehydes, one of the products of lipid peroxidation, can alkylate bases [67] or form intra- and inter-strand cross-links [68].

2.4.4.3 Charged particles

Mendis et al. [69] and Laroussi et al. [42] suggested that the charged particles play an important role in the inactivation process (demonstrated to date only for gram-negative vegetative bacteria). Charged particles coming from plasma accumulate on the outer cell membrane and exert electrostatic force due to the repulsive forces, which leads to lysis of the cell as a result of the rupture of its membrane.

Laroussi et al. [70] and Sun et al. [71] supported this conclusion by direct exposure experiments. The SEM micrographs of *E. coli* after treatment show the membrane disruption. Lu et al. [72] studied the role of the charged particles in the inactivation process by using a thin wire to collect the charged particles. They found that the charged particles play a minor role in the inactivation process when He/N_2 (3%) is used as working gas. While He/O_2 (3%) is used, the charged particles are expected to play an important role in the inactivation of bacteria and the negative ions O_2^- might be the responsible charged particles. Shi et al.[73] supported this conclusion by the TEM examination of Candida albicans and protein, nucleic acid and K^+ leakage detection after treatment. Fridman et al.[74] drew the same conclusion by comparing direct and indirect influence on microorganisms of non-thermal atmospheric-pressure DBD in air.

However, other researchers showed that charged particles play a minor role in the destruction of microorganism. Deng et al. [75] used *Bacillus subtilis* spores as a model and an atmospheric-plasma plume in helium flow, optical emission spectroscopy and inactivation kinetics to demonstrate the dominating role played by the reactive oxygen species (e.g., atomic oxygen and OH) as well as the minor contributions of charged

particles. Kim et al.[76] had the same conclusion from the survival curve of *E. coli*. Park et al. [77] treated *E. coli* and S. aureus by microwave argon plasma and observed rupture of them by SEM. According to the authors, the rupture is due to a strong etching process caused by UV emission.

2.4.5 Sub-lethal study: spore germination after plasma treatment

Plasma can induce sub-lethal changes that are functional changes to cells without actually killing them. Laroussi et al. [78] investigate the effects of plasma exposure on the biochemical pathways of Gram-negative (*E. Coli*) and Gram-positive bacteria (*B. subtilis*) and determined whether exposure to plasma alters the heterotrophic pathways of the bacteria by sole carbon substrate utilization (SCSU) experiments. They reported changes in metabolism indicating significant changes in the corresponding enzyme activities without inducing any lethal impact on the cells [78]. Sub-lethal study on spore germination after plasma treatment helps us to understand what kinds of changes induced to spores by plasma that make them malfunction without killing them.

2.5 Investigation of biochemical changes in bacterial spores by Fourier transform infrared spectroscopy

Fourier transform infrared (FTIR) spectroscopy combined with chemometric methods was used to quantify viable spores and identify some biochemical changes in samples treated by autoclave [79], pressure-assisted thermal processing (PATP) [12, 13], and thermal processing (TP) [12, 13], providing an accurate analytical tool for

understanding mechanisms of sterilization techniques in inactivating bacterial spores.

Helm et al. [80] detected and identified some particular cell components by FTIR of intact bacteria and typical marker bands were used to identify these bacterial cell components.

Perkins et al. [79] utilized FTIR to identify cellular components, or bio-markers of spores. There are considerable changes that occur in the amide I and II regions in samples that have undergone autoclaving indicating secondary structure conversions to intermolecular β -sheet due to protein denaturing and subsequent aggregation during the autoclaving process [79]. Dipicolinic Acid (DPA) undergoes undetermined transformation as indicated by DPA bands [79].

Subramanian et al. [13] reported that changes of spectral wavenumbers 1655 cm^{-1} and 1626 cm^{-1} indicating spores structure changes of α-helix and β-sheets of secondary protein during PATP. Subramanian et al. [13] concluded that release of DPA during the initial stages of PATP was evident in that infrared absorption bands from DPA (1281, 1378, 1440, and 1568 cm^{-1}) decreased significantly. While during TP, the bands associated with secondary proteins shifted and DPA bands showed little or no change. A correlation was found between the spore's calcium dipicolinate (Ca-DPA) content and its resistance to PATP [13]. By comparison of spectra of treated spores and untreated ones, the information of subtle biochemical changes during the process was obtained.

2.6 Real time monitoring of spore germination by attenuated total reflection Fourier-transform infrared spectroscopy

Chueng et al. [81] monitored chemical changes of particular *Bacillus subtilis* spore components by attenuated total reflection Fourier-transform infrared spectroscopy (ATR-FTIR) during spore germination on a ZnSe internal reflection element. They reported that significant changes in the amount of Ca-DPA and proteins were observed in the wild-type strain, as well as the germination mutant (strain 1G9, gerD) but with a slower rate. In contrast, germination of another mutant (strain 167, gerA) was slow and incomplete, and proteins and Ca-DPA remained the same during the germination study [81]. This technique provides substantial value for monitoring changes in the functional groups of molecules inside the cells during germination and can be applied to the germination and sub-lethal study in chapter IV.

CHAPTER III
Inactivation Mechanisms of *Bacillus amyloliquefaciens* spores by Non-thermal Plasma

Abstract

Inactivation of *Bacillus amyloliquefaciens* (BA) spores by non-thermal plasma (NTP) was investigated by studying inactivation kinetics and using attenuated total reflection Fourier-transform infrared spectroscopy (ATR-FTIR). ATR-FTIR is a useful tool to probe the biochemical and structural changes of spores after NTP treatment in order to better manipulate and optimize the parameters for NTP processing. The microdischarge generated by the dielectric barrier in our research has higher energy efficiency compared with a uniform glow discharge at atmospheric pressure and autoclave. The survival curve showed two phases with different spore inactivation rates and changes in surface topography of the spores assessed by atomic force microscopy (AFM) indicating that NTP treatment disrupted spore aggregates so that reactive species could reach and inactivate the bottom layers of spore films. Scanning electron microscopy (SEM) images showed that the spore surface was etched away after NTP treatment. Multivariate classification models based on Soft Independent Modeling of Class Analogy (SIMCA) were developed to identify the biochemical changes after NTP treatment. The absorbance of bands correlated to dipicolinic acid (DPA) ring decreased after NTP treatment indicating that DPA released and then reacted with reactive species generated by plasma, which was confirmed by NMR spectra. Also bands corresponding to protein structure changed after NTP treatment.

3.1 Introduction

Spoilage caused by spores often results in large economic losses and has become a prime concern in the food industry. The spore-forming nature of certain bacteria enables them to exhibit high resistance to various environmental stress factors including: (i) moist heat; (ii) osmotic, nitrite-, and pH-induced stress; (iii) prolonged frozen storage; and (iv) high hydrostatic pressure, then germinate and grow, leading to spoilage of food products and even food poisoning outbreaks[6]. Efficient spore inactivation approaches are needed to meet consumer expectations for increased food safety, extended shelf life and improved food quality. Furthermore, as some biowarfare agents are spore-forming bacteria, anthrax, for example, development of spore inactivation technologies may also lead to an effective response to bioterrorism [2-4].

Non-thermal plasma is a developing method to efficiently kill microorganisms. Plasma most commonly used for sterilization is known as cold plasma, or non-thermal plasma with reference to its gas temperature [10]. They are neutral ionized gases that constitute not only ions and electrons, but also uncharged particles including photons, atoms, reactive species, and excited or non-excited molecules. Non-thermal plasma is efficient and economically viable due to relatively low installation costs and energy consumption. So it is regarded as a potential alternative to conventional sterilization methods used in food processing and sanitizing heat susceptible materials because of its non-thermal feature.

Attenuated total reflection Fourier-transform infrared spectroscopy (ATR-FTIR) is an easy and sensitive technique providing structural and chemical information at the molecular level. Some cellular components of bacteria can be identified by infrared

spectroscopy [12], and constituents such as lipids, dipicolinic acid (DPA) and intracellular materials have been detected with this method [13].

In this chapter, mechanisms of spore-inactivation were determined by studying inactivation kinetics and using ATR-FTIR to probe the biochemical and structural change after NTP treatment. This study will contribute to optimizing the parameters for non-thermal plasma processing.

3.2 Materials & Methods

3.2.1 Spore preparation

Bacillus amyloliquefaciens (BA) spores were activated in ST1 liquid medium (Merck, St. Paul MN) at 30 ℃ for 24 hours. Aliquots (0.1 mL) from fresh overnight cultures were plated on ST1 agar plates supplemented with 10 mg/L $MnSO_4 \cdot H_2O$ which stimulates vegetative cell growth. The agar plates were incubated aerobically at 30 ℃ for 5 days. During incubation, spores germinated to vegetative cells first and replicated, then vegetative cells sporulated due to starvation with less nutrition left. Spores were collected and enriched from the plates following the protocol described in [82] by flooding the surface with cold sterile distilled water and collecting the rinsate. The suspension was washed twice by sterile distilled water: suspension was centrifuged at 10000 RPM for 10 min, and then dumped supernatant and resuspended in sterile distilled water. Washed pellets were suspended in 0.05 mol/L potassium phosphate (pH=7.0) containing lysozyme (100 μg/mL), and incubated with stirring at 37 ℃ for 1 hour to digest cell walls

of vegetative cells [83]. After digestion, enzyme treated spores were washed with distilled water four times to remove vegetative cell debris and store at -15 ℃ until use.

3.2.2 Plasma generation and energy consumption measurement

The non-thermal plasma (NTP) was generated by the dielectric barrier discharge (DBD) as shown in Figure 3-1.

The upper dielectric barrier is made of polyacrylic acid and a glass slide loaded with spores was used as the lower dielectric barrier. Metal electrodes (aluminum tapes) were attached to each dielectric barrier. One electrode was connected to the high voltage power supply; the other was connected to the ground. Non-thermal plasma was generated in the gap between two dielectric barriers, with a large number of microdischarges randomly distributed. If not specified, NTP in this study used air as feed gas. A capacitor was connected in series in the circuit and used to measure power following the Equation 2 as mentioned in section 2.4.2.

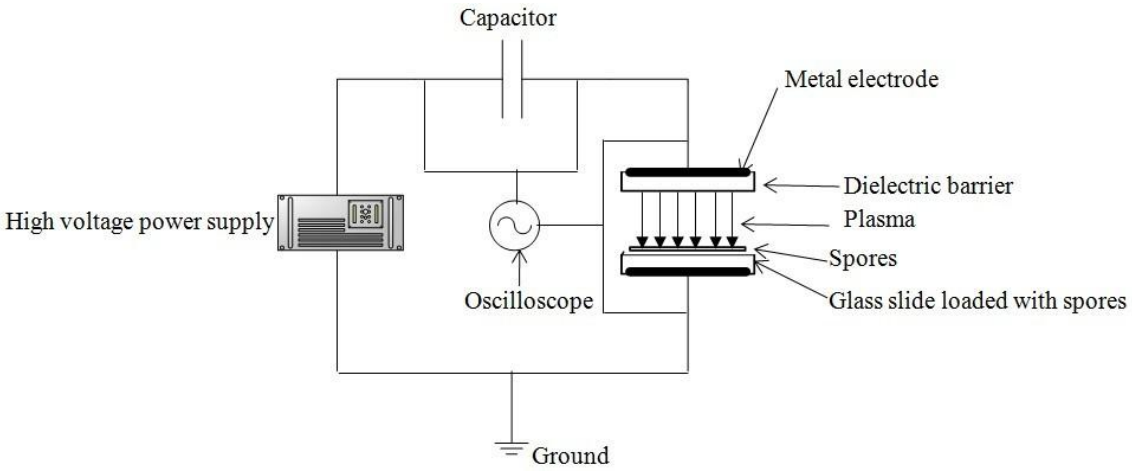


Figure 3- 1 Schematic diagram of plasma generation by dielectric barrier discharges

The area of the Lissajous figure display on the oscilloscope is equivalent to the energy dissipated during one period [39]. The measured plasma power density was used to describe energy consumption per unit area equivalent to power/volume. The dimension of the metal electrode was 25.5 mm x 25.5 mm.

3.2.3 Plasma inactivation kinetics

Aliquots of BA spore suspension (100μL) were spread onto glass slides and dried at room temperature, forming a 20mm*25.4mm spot. Each glass slide loaded with spores was placed in the plasma chamber at a distance of 2.6mm away parallel to the upper dielectric barrier and was NTP treated for specified time lengths up to 8 min. After exposure, spores were washed from the glass slide by 1mL water and serially diluted. Each dilution was sampled for 100μL three times and each sampling was spread on ST1 broth agar plate. Inoculated plates were incubated at 30 ℃ for 24 hours and the resulting colony forming units (CFU) was counted to determine the inactivation efficiency.

3.2.4 Spore morphology observation

Spore suspensions (100μL) were diluted to 6 $\log_{10}$CFU/ mL in order to have better observation and spread on the silicon specimen chip supports attached to the scanning electron microscopy (SEM) pins via copper tape. With the low electrical resistance and surface properties better than glass, silicon chip specimen supports are ideal for mounting cells and imaging small particles due to low background signal. Spore suspensions with or without drying in room temperature prior to NTP treatments of 1, 3, or 5 min were prepared along with untreated control samples. Samples was coated with gold by vacuum

evaporation and observed with SEM (Zeiss 1525, Carl Zeiss SMT Inc.). NTP treatment was repeated as above and spores after NTP treatment were washed from the chip by 1 mL distilled water, which was plated to the ST1 agar plate immediately and checked spore viability after 24 hour.

3.2.5 Spore surface analysis by atomic force microscopy

Spore suspensions were diluted to 6 $\log_{10}$CFU and spread on two silicon chips. After spores dried at room temperature, one chip was put in the plasma chamber to receive 1min plasma treatment and another chip was used as control. The topography of spore surface was examined using an atomic force microscopy (AFM) with non-contact mode. The scan area size was 10μm*10μm and the scan rate was 1.00 Hz.

3.2.6 Attenuated total reflection Fourier-transform infrared spectroscopy analysis of spore after NTP treatment

FTIR spectra were recorded using a FTIR spectrometer (Excalibur 3100, Varian Inc. Palo Alto, CA) equipped with a liquid nitrogen cooled mercury cadmium telluride (MCT) detector. The sampling station was equipped with an overhead Attenuated Total Reflection (ATR) accessory with germanium crystal (PIKE Technologies, Madison WI). Spore suspensions were spread on four plates and dried at room temperature. Three plates were treated by NTP as described in 3.2.2 for 1, 3, or 5 min, and one plate was used as untreated control. A part of spore powders scraped from the plate were placed on the KBr plate and pressed for FTIR scanning. After one scan, loaded spores powders were mixed with spores powders scraped from the same plate and a part of the mixture was loaded for the next measurement. FTIR spectrum of each plate was measured 15 times. Each FTIR

spectrum was collected in the mid-IR region from 1800-1000 cm^{-1}, which is the fingerprinting region for microorganisms, at a resolution of 4 cm^{-1} after averaging 128 scans. Single reflection spectra of samples which detected all signals of samples due to tight contact were obtained and presented in absorbance units after taking into account the background spectrum of air. The ATR crystal (made of Germanium) was carefully cleaned with ethanol, distilled water, and dried between successive measurements to prevent cross contamination. Spectra were baseline corrected and ATR corrected by Thermo scientific OMNIC software (Thermo scientific, Waltham MA).

Multivariate analyses of the data were performed using the chemometrics modeling software Unscrambler 9.2 (CAMO Software Inc., Woodbridge, NJ). For analysis, spectra were imported into Unscrambler, mean-centered, and vector-length normalized. Discrimination of the spores with different treatment time was carried out using classification analysis based on soft independent modeling of class analogy (SIMCA). The data were projected onto principal component axes to visualize clustering of the four groups of spores with different treatment time. The discriminating power plots provided by SIMCA were used to identify the infrared bands that were responsible for differentiating spores with different treatment time and to determine the biochemical changes in the spore composition after NTP treatment.

3.2.7 Nuclear magnetic resonance analysis of DPA

Nuclear magnetic resonance analysis (NMR) analysis of DPA left in spores was employed to validate the conclusion drawn by FTIR spectra, following the protocol developed by Loshon, et al. [84]. NTP treated and untreated spores were boiled in water

respectively (1 mL) for 30 min. The extracts were cooled on ice and centrifuged, and the pellet was washed twice with 1 mL of water. The pooled supernatant fluids were passed through a 1-mL Chelex column in water at room temperature to remove divalent cations, the column was rinsed with 2 mL water, and the column washes were pooled and lyophilized. The dry residue was dissolved in 700 mL of D_2O, and t-butanol was added (0.5μL) to serve as an internal standard. The solution was then subjected to nuclear magnetic resonance (NMR) spectroscopy with a 300 MHz Varian Inova NMR spectrometer (Varian Inc. Palo Alto, CA). VNMR software (Varian Inc. Palo Alto, CA) supported data acquisition, processing, and display. Data was processed by Mestrenova software (Mestrelab Research, Santiago de Compostela Spain).

3.3 Results and Discussion

3.3.1 Kinetics of plasma inactivation of BA spores

The inactivation efficiency of NTP treatment was determined by measuring the survival of spores using viable plate count method and the results are shown in Table 3-1. The data point of treatment time equals to 8 min deviated from the data set because the determine limit of the serial dilutes method is 1 $\log_{10}$CFU. A bi-slope survival plot was observed (Figure 3-2). In this study, preliminary experiments showed that kinetic curve cannot be drawn by using low spore concentration as initial control because the killing process is so fast that the CFU of surviving spores cannot be captured in such short time intervals. So compared with other studies, a much higher concentration of spores was used. During the first phase, the inactivation rate was high with 3.90 $\log_{10}$ CFUs/mL/min and the $\log_{10}$CFUs of survival spores decreased from17.12 $\log_{10}$CFUs/mL to 5.31

log_{10}CFUs/mL and achieve sterilization (about 12 log_{10}CFU/mL reductions) in 3 min. The D-value (time required to inactivate 90% of the spores) of the first phase was 0.165 min. The inactivation rate decreased in the second phase (from 3 to 8 min) to only 0.9178 log_{10}CFUs/mL/min. Spore growth was not detected after 8 min of N treatment. Single- [41-43], bi- [44, 45] and multi-slope [46, 48, 49] survival curves have been reported on the germicidal effects of non-thermal, atmospheric pressure plasmas. The different patterns of survival curves previously reported is likely due to variations in the experimental devices and physicochemical conditions previous researches produced during the inactivation process. The bi-slope survival curve observed in our study likely occurred because NTP inactivation was only a surface treatment, thus resulting reactive species such as ozone and other oxidants were initially unable to penetrate spores in the bottom layers. Cell debris accumulation during the rapid initial inactivation phase leads to a slower secondary inactivation phase.

Table 3- 1 Kinetics data of plasma inactivation

time	Mean (n=3)	std.
0	17.12446	0.04475
0.5	14.38085	0.027071
1	13.21089	0.052807
1.5	10.6593	0.066597
2	8.75075	0.058162
2.5	6.997075	0.150536
3	5.314465	0.032535
3.5	4.525953	0.057279
4	4.20109	0.040151
4.5	3.933477	0.075639
5	3.396777	0.095171
5.5	2.96064	0.045103
6	2.578442	0.042096
6.5	2.185764	0.032633
7	1.827646	0.123538
7.5	1.407953	0.043146
8	0	0

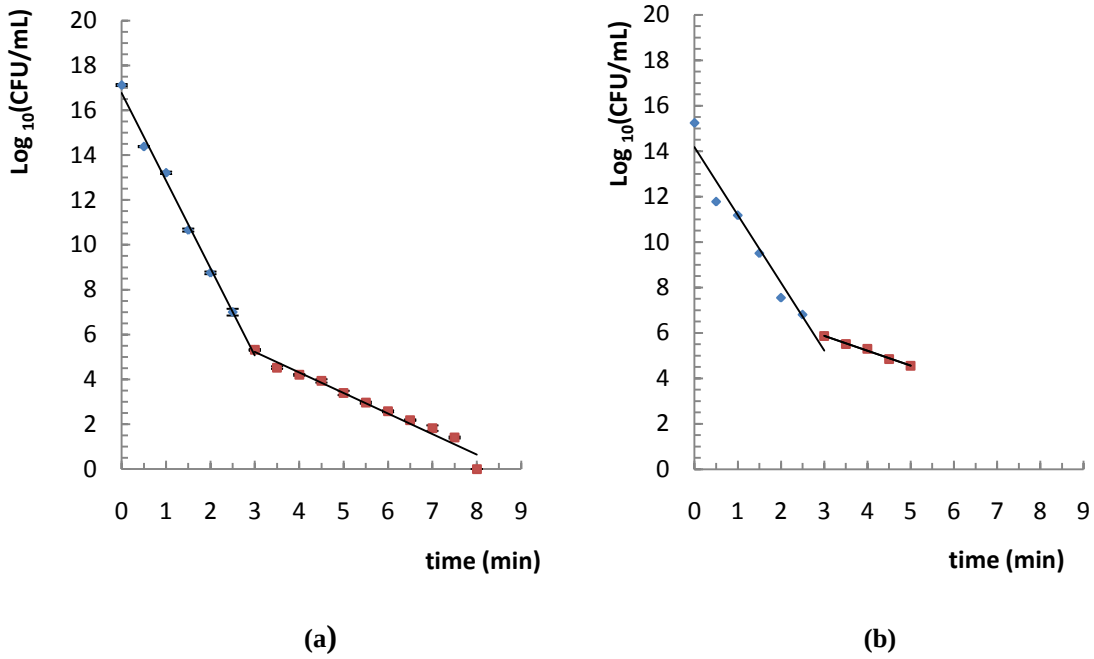


Figure 3- 2 Survival plots of spores after NTP treatment for different times (a) and preliminary data with different initial concentration and few time points (b).

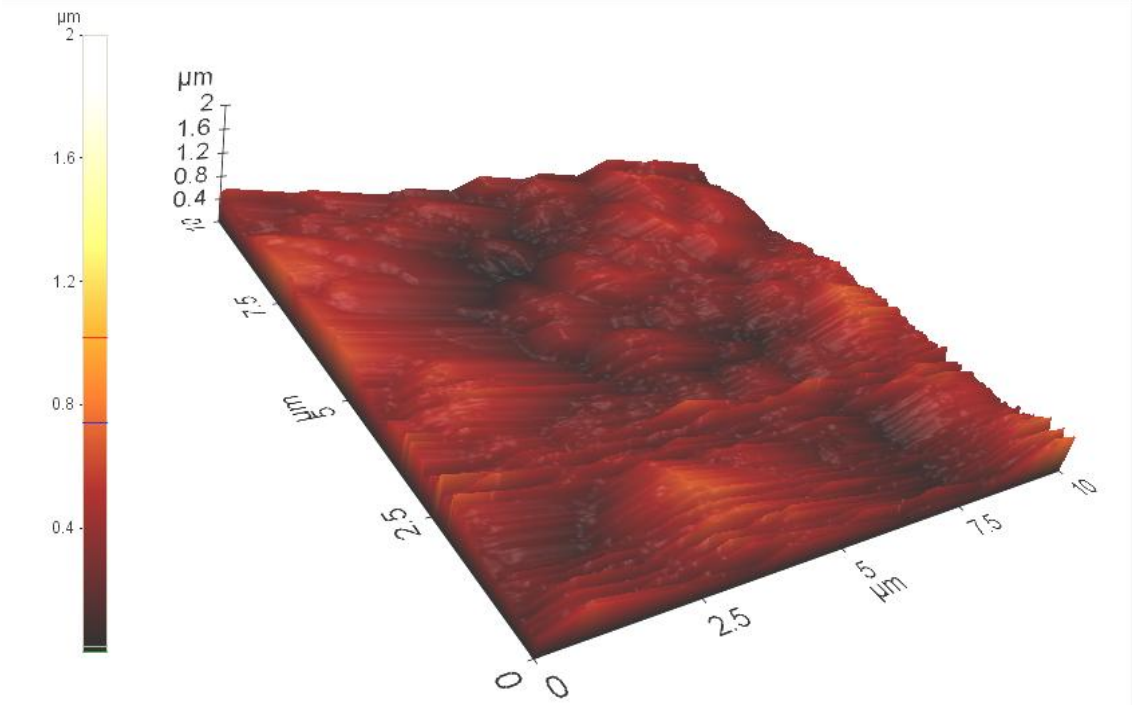
The equation of the straight line of first phase relating $\log_{10}$CFU and time is estimated as: $\log_{10}$CFU = (16.7759) + (-3.9041)*time using the first 7 time points in this dataset. The y-intercept, the estimated value of $\log_{10}$CFU when time is zero, is 16.7759 with a standard error of 0.2382. The slope, the estimated change in $\log_{10}$CFU per unit change in time, is -3.9041 with a standard error of 0.1321. The value of R-Squared, the proportion of the variation in $\log_{10}$CFU that can be accounted for by variation in time, is 0.9943. The correlation between $\log_{10}$CFU and time is -0.9971.

A significance t-test (NCSS 2007, Kaysville UT) that the slope is zero resulted in a t-value of -29.5509. The significance level of this t-test is 0.0000. Since 0.0000 < 0.0500, the hypothesis that the slope is zero is rejected.

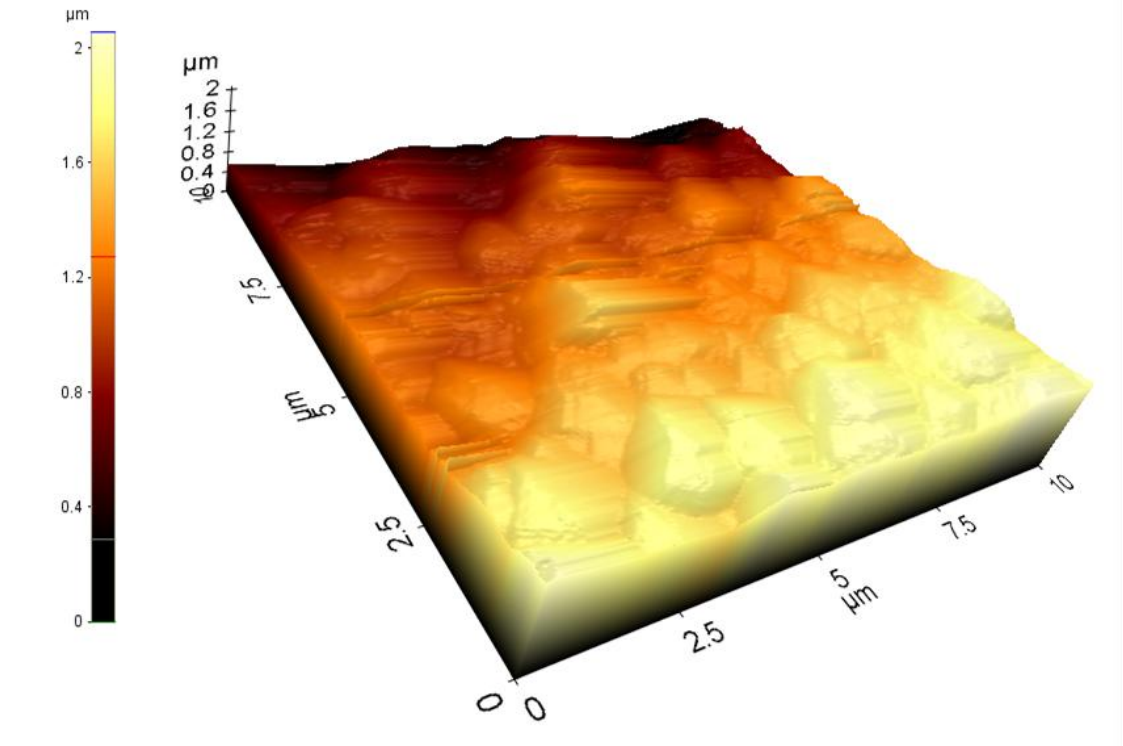
The equation of the straight line of second phase relating $\log_{10}$CFU and time is estimated as: $\log_{10}$CFU = (7.9871) + (-0.9178)*time using the 11 time points in this dataset. The y-intercept, the estimated value of $\log_{10}$CFU when time is zero, is 7.9871 with a standard error of 0.3050. The slope, the estimated change in $\log_{10}$CFU per unit change in time, is -0.9178 with a standard error of 0.0533. The value of R-Squared, the proportion of the variation in $\log_{10}$CFU that can be accounted for by variation in time, is 0.9705. The correlation between $\log_{10}$CFU and time is -0.9852.

A significance t-test (NCSS 2007, Kaysville UT) that the slope is zero resulted in a t-value of -17.2189. The significance level of this t-test is 0.0000. Since 0.0000 < 0.0500, the hypothesis that the slope is zero is rejected.

The topography of the spore surface (Figure 3-3) confirmed the explanation for bi-slope survival. The spores stack height difference of control spore surface was 600nm (we changed the scale of Z axis to 2μm for better comparison) while it was 2μm in the 1 min plasma treated spore surface. The height difference of control spore surface equaled the height of a single spore. During NTP treatment, upper layer spores reacted with reactive species and were etched away randomly by the microdischarge. The plasma might have static force on the multi-layered spores and continued to disintegrate the spore stack such that the reactive species could reach the bottom layers of spores to inactivate them, albeit, at a slower rate.



(A)



(B)

Figure 3- 3 Topography images of spore surface difference: (A) control; (B) plasma treated for 1 min

3.3.2 Energy consumption in NTP treatment

The device was operated at 2200 V. The energy consumption of non-thermal plasma, excluding the energy emitted by other forms, such as heat, etc., is equal to the area of the ellipse (the integral of the Lissajous figure in Figure 3-4) times the frequency of the power and capacitance. Given frequency equals 28.9878 kHz, C (capacitance) equals 0.001μF, area of the ellipse equals $3.316*10^4$ V^2, and the power of discharge equals 0.961w. The plasma power density calculated following:

$$\text{Power density} = \text{power}/\text{discharge volume} \qquad \text{Equation 5}$$

Plasma density of device which was used in this study equals 0.568w/cm^3.

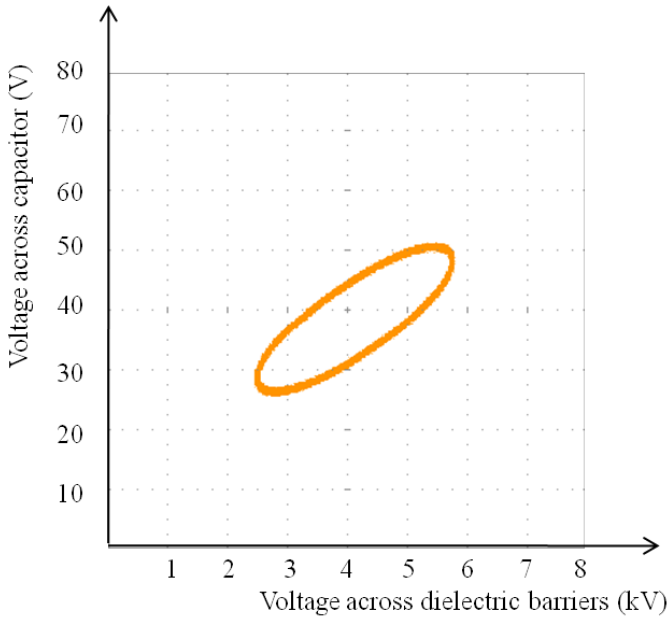


Figure 3- 4 Lissajous figure of discharge

Unlike the stable and uniform glow discharge at atmospheric pressure (GDAP), which is a single pulse per half cycle with a slow decay time [42], the microdischarge is made of a large number of filamentary discharges and exhibits a current with multiple sharp pulses each half cycle. Compared with the GDAP, the plasma power density of microdischarge is 5 to 10 times higher according to Laroussi's research [42], because the feed gas of GDAP, helium, is easier to ionize than air with lower ionization energy. However, the energy efficiency of GDAP is not as high as microdischarge, which takes 20 min to achieve a 5 $\log_{10}$CFU reduction [42] and the energy consumption is 68.16J/cm^3 (0.568/10*20*60 J/cm^3), while microdischarge of our device takes only 1.3 min and the energy consumption is 44.30 J/cm^3 (0.568*1.3*60 J/cm^3). Besides, helium is much more expensive than air.

To compare energy consumption with autoclaving, given an autoclave with chamber dimension of 22.6 cm width, 45.7 cm diameter and power equal to 1750w, and assuming it can autoclave 1/3 of its volume, the power density of autoclave equals 0.142w/cm^3. However, autoclave takes about 30 min to achieve 5 $\log_{10}$CFU reductions and the energy consumption is 255.6 J/cm^3 (0.142*30*60). So the energy consumption of NTP treatment is lower and microdischarge has the best energy efficiency compared with GDAP and autoclave.

3.3.3 Morphology observation

The various treated and untreated spore samples exhibited different surface textures (Figure 3-5). Control spores were intact and oval shaped, with smoother surfaces (Figure

3-5A), as compared to the treated spores exhibited a rough surface damaged after 1 min of NTP treatment (Figure 3-5B). After 3 min treatment, the surface became rougher and the outer layer was almost completely etched away (Figure 3-5C). As the treatment time increased to 5 min, the outer membrane of the spore was totally destroyed and holes were observed in the inner membrane (Figure 3-5D). SEM images showed that one mechanism of spores inactivation by plasma is to etch away coats and cortex of spores, and even deeper into the core. Subsequent germination and growth of the spores on nutrient media was only observed for the control and 1 min treated samples.

No survival was observed after plating wet spore (Figure 3-5 E, F) samples on nutrient media that had been treated with plasma. The presence of water clearly enhanced the inactivation efficiency of NTP treatment as some spores survived the shorter treatment intervals of dry samples. Two possible mechanisms are proposed here: first, in the 1 min wet treated sample, the spore membrane appeared to be peeled off rather than randomly etched away in the dried sample. It is possible that charged particles coming from plasma accumulate on the outer membrane with the spore suspension acting as conductor and exerting electrostatic force due to the repulsive forces, leading to rupture of the spore; second, the water vapor could react with the plasma, forming OH ·radical, a highly reactive species, having extremely high rate-constants for reactions with almost every type of molecule found in living cells [53]. At the same time, we observed that some chemicals were released by the spore and dissolved in the water, which cannot be seen in the dry samples. In the 3 min treated samples, the water evaporated within one and half minutes and the surface was randomly etched away as in the samples that were dried prior to treatment.

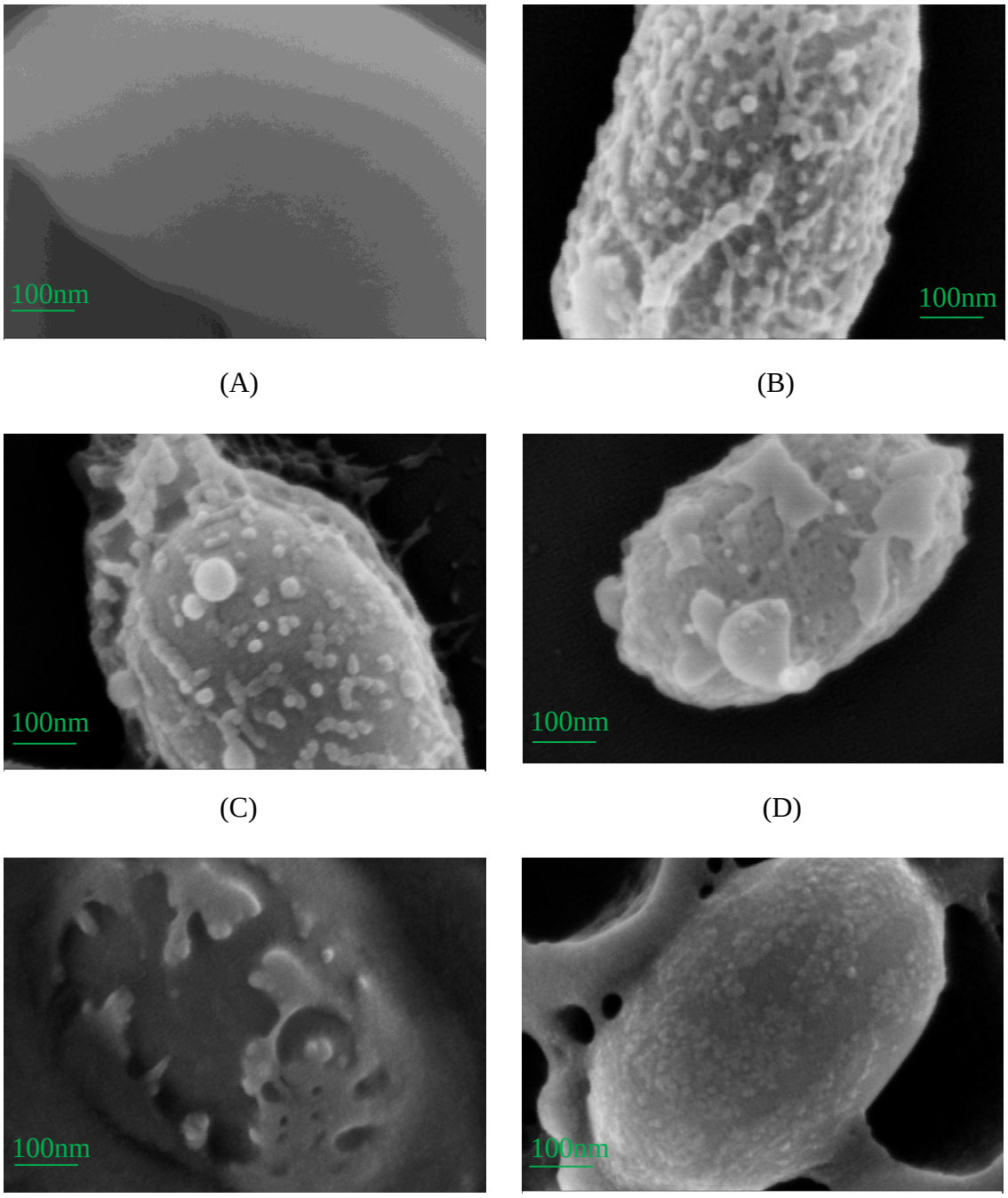


Figure 3- 5 SEM imaging: (A) Dried control, (B) Dried spores plasma treated for 1 min; (C) Dried spores plasma treated for 3 min; (D) Dried spores plasma treated for 5 min; (E) Wet spores plasma treated for 1 min; (F) Wet spores plasma treated for 3 min.

3.3.4 Fourier transform infrared spectroscopy analysis

Functional group assignments of spore components and protein structures are shown in Table 3-2. Comparison of ATR-FTIR spectra of spores before and after NTP treatments (Figure 3-6) showed significant biochemical changes, especially DPA and secondary protein structures. The spectrum of control group had higher absorbance than the plasma treated groups. However, peaks in spectra without chemometric processed were not sharp enough to delineate significant change after NTP treatment. A discrimination power plot was used to identify the spectral wavenumber and associated functional groups that had significant differences in SIMCA class projections. Higher values of discriminating power indicate greater influence of those wavenumbers in classifying the samples with greater differences. Four distinct clusters corresponding to the control and plasma treated samples with different treatment time were well separated in 3D space of the SIMCA class projection plot (Figure 3-7).

Table 3- 2 Assignment of Bands in the FT-IR Spectra of Bacterial

Wavenumber (cm^{-1})	Functional group assignment
~1656	Amide I band of α-helical structure of secondary proteins [12]
~1630	Amide I band of β-pleated sheets of secondary proteins [79, 85, 86]
~1626	Amide I band of β-pleated sheets of secondary proteins (shifted because of autoclaving) [79]
~1616	Stretching bands of COO^- group of DPA-Ca chelate [12]
~1605	Symetrical carboxylate stretching vibrational bands [80]
~1570	C-N vibrations of the DPA ring [79]
~1558	Amide I band (primarily a C=O stretch) [79]
~1535	Amide II polypeptide structures [79]
~1515	Tyrosine bands [87]
~1440	Bands of acid peptides [81]/DPA pyridine ring vibration [88, 89]
~1410	C-O-H in-plane bending of lipids, carbohydrates, and proteins [12]
~1378	Stretching bands of COO^- group of DPA-Ca chelate [80]
~1350-1320	C-N stretch band [90]
~1280	Amide III bands of proteins [80, 91]/DPA band [79]

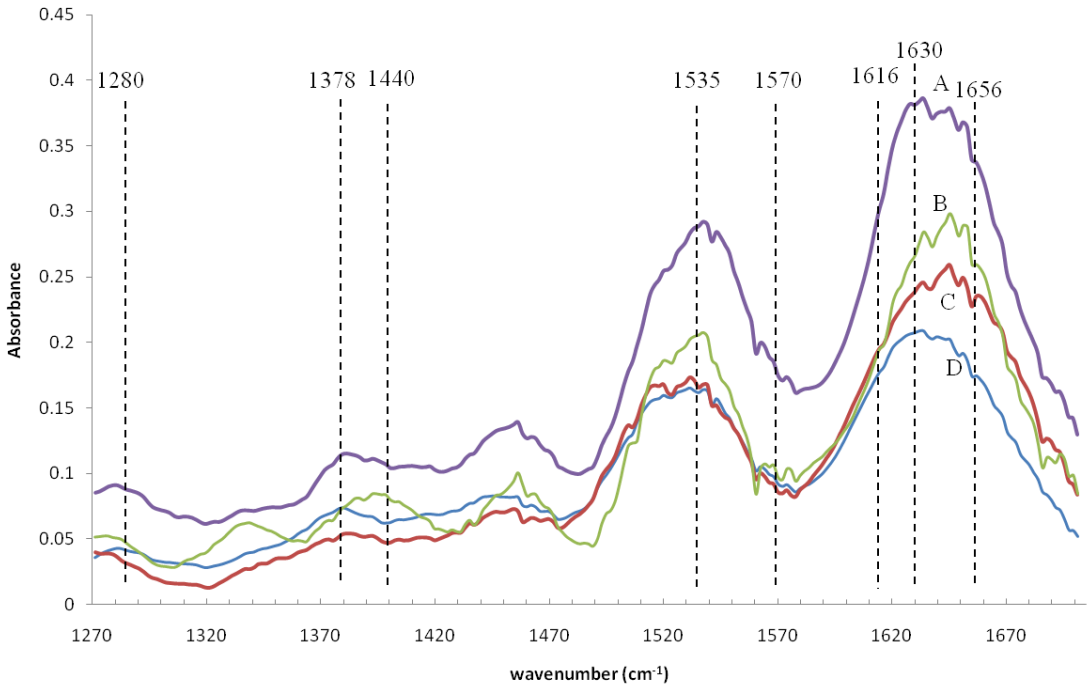


Figure 3- 6 ATR-FTIR spectrum of spores: (A) control; (B) 1 min plasma treated; (C) 3 min plasma treated; (D) 5 min plasma treated

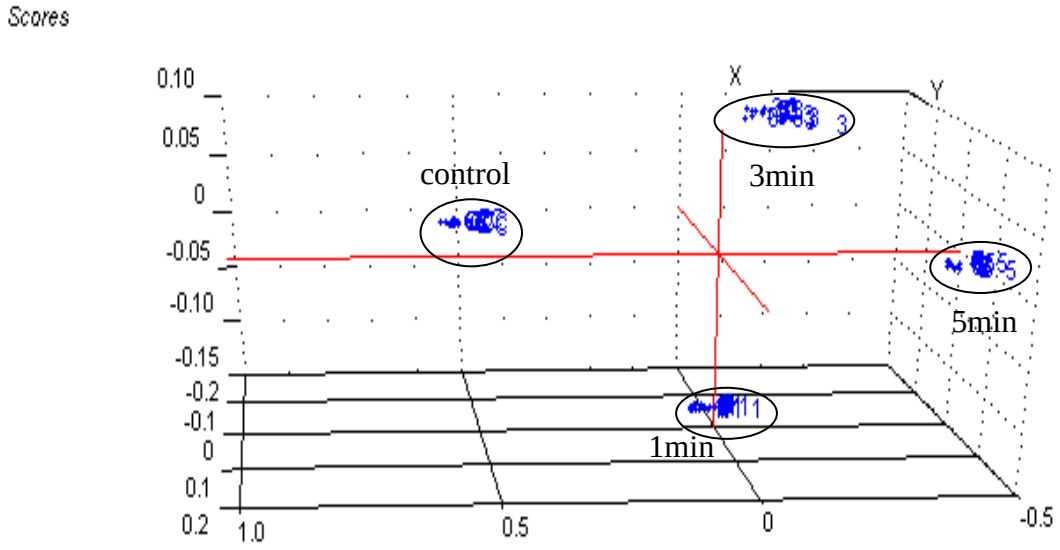


Figure 3- 7 Soft independent modeling of class analogy class projections of spores under different treatment time

According to the discriminating power plot (Figure 3-8) and the original FT-IR spectra (Figure 3-6), both bands at 1280 cm^{-1} (DPA and amide III bands) and 1440 cm^{-1} (DPA pyridine ring vibration and acid peptides bands) decreased after NTP treatments but not very significant because they are not only correlated with DPA, but also responded to other biochemical structure. Stretching bands of COO^- group of Ca-DPA chelate (1616 cm^{-1} and 1378 cm^{-1}) [12] also slightly decreased, but they also shifted because new COO^- groups were formed due to oxidation caused by reactive species. The C-N vibrations of the DPA ring band (1570 cm^{-1}) also decreased, indicating the ring structure of DPA was broken. As peaks assigned to DPA lost intensity compared with control group, it is possible that DPA was released and then reacted with reactive species generated by plasma during the NTP treatment. DPA plays an important role in spore resistance and signal transduction in spore germination so that the loss of DPA caused by plasma will have a critical impact on spore germination and their resistance to harsh environment.

Bands at 1535 cm^{-1}, 1630 $cm^{-}1$, and 1656 cm^{-1}, corresponding amide II polypeptide structures , amide I bands of β-pleated sheets of secondary proteins [85, 86] , and amide I band of α-helical structure of secondary proteins [12], respectively, also decreased in the plasma treated samples and band 1656 cm^{-1} was shifted after NTP treatment. Poly-glutamic acid, which is the major component of the spore wall, preferentially forming α-helical structures was believed to be responsible for the strong α-helix band at 1656 cm^{-1} [80] and band shifts and changes was due to protein denaturing and subsequent aggregation [79] during NTP treatment. Also tyrosine band at 1515 cm^{-1} [87] that down shifted to 1500 cm^{-1} indicating proteins upon aggregation, which has been suggested as

indicative of stronger hydrogen bonds of the tyrosine OH group with acceptors in the protein aggregates [92].

The spectrum indicated that plasma destroyed spore coats and membranes supporting the morphological changes observed in SEM images of treated spores.

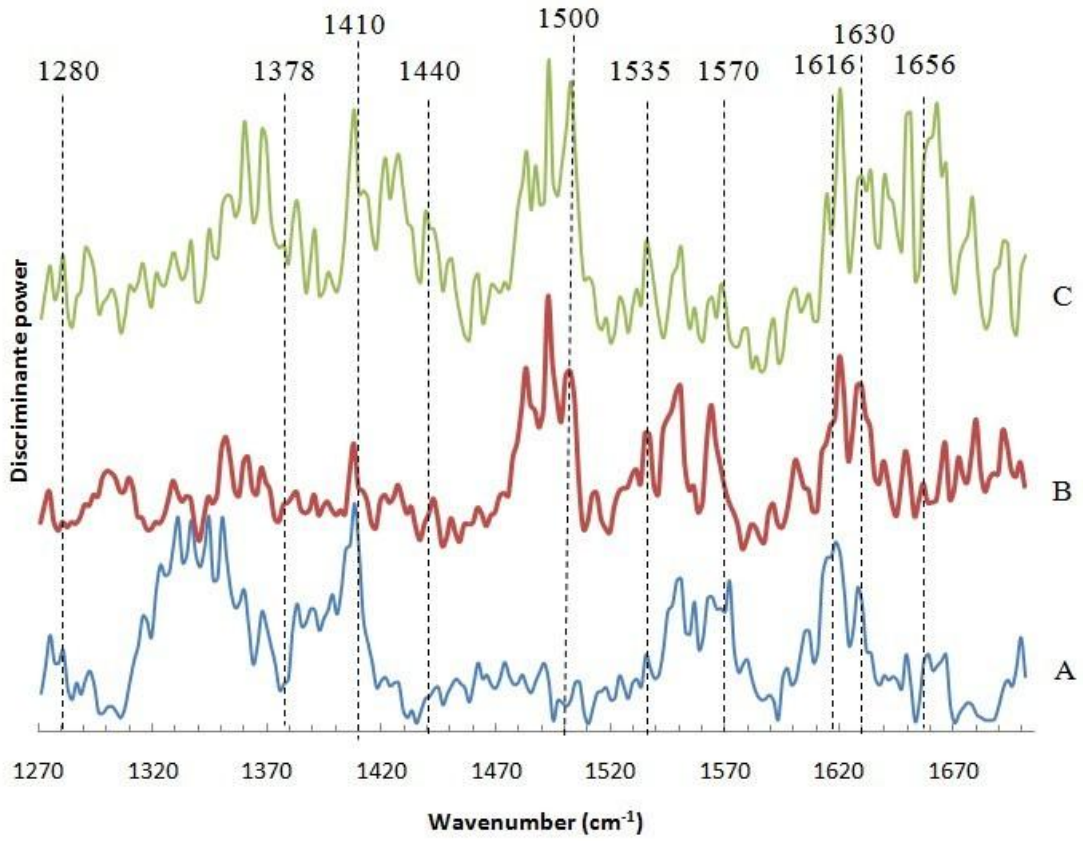


Figure 3- 8 Discriminating power in classification of treated spores with control. Prominent bands and their relative to importance in discriminating control and (A) 1 min; (B) 3 min; (C) 5 min plasma treated spores.

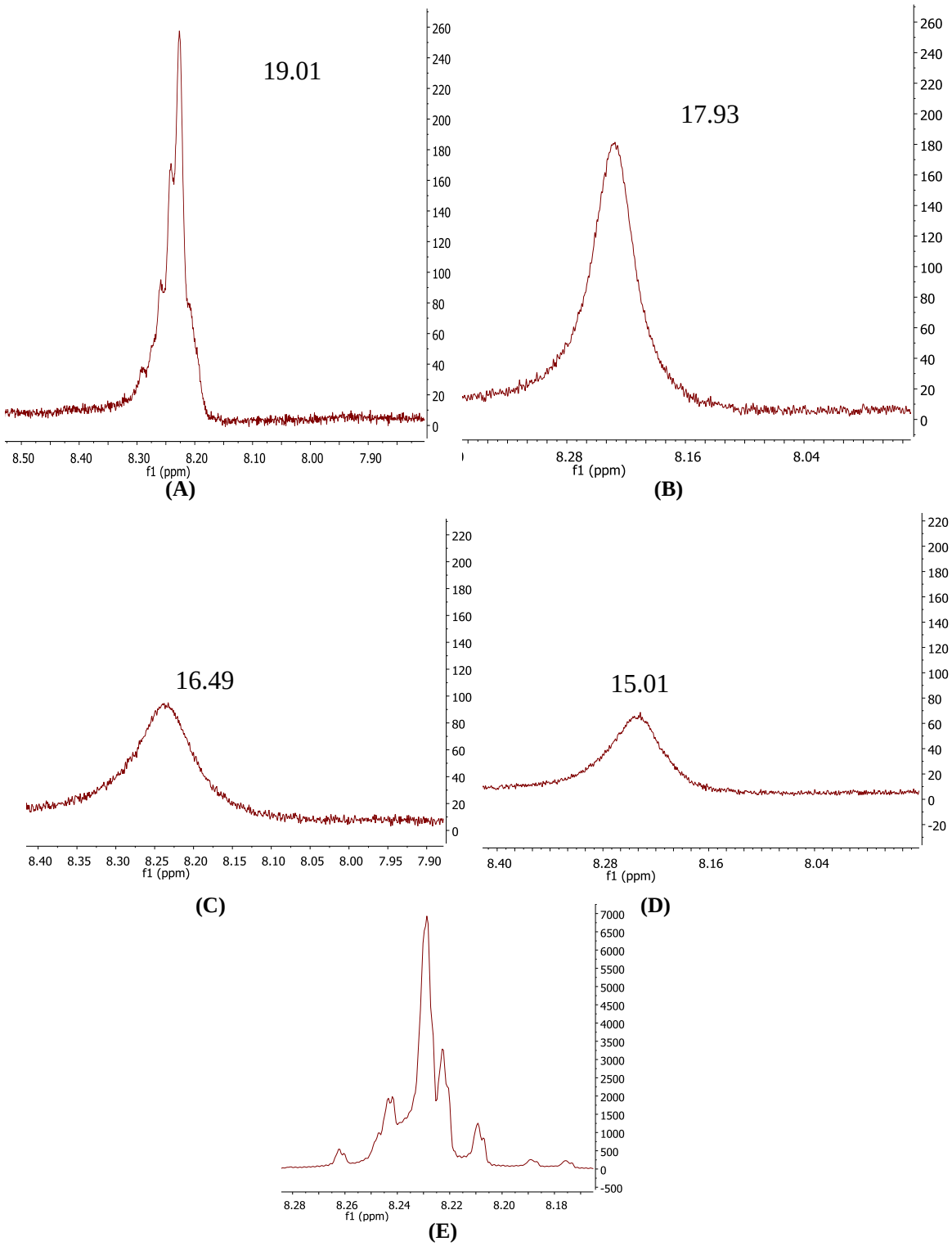


Figure 3- 9 ^{1}H NMR spectrum of spore extraction: (A) control; (B) 1 min; (C) 3 min; (D) 5 min; (E) standard DPA. Numbers were normalized integrals of DPA peaks.

3.3.5 NMR analysis of DPA

Proton peaks corresponding to DPA were indentified in NMR spectra of spore extracts as indicated by a chemical shift of DPA peak (8.24 ppm). DPA peaks of treated spores appeared in the same position as control, indicating DPA structure remained the same after NTP treatment (Figure 3-9). However, the amount of DPA remaining in the core of spores changed after NTP treatment. The proportion of DPA peaks to t-butanol (used as an internal standard) decreased as treatment time increased, which indicated the amount of DPA decreased. DPA content of spores treated for 5 min was reduced by 21.04% compared with the control. The results confirmed that DPA was released and then reacted with reactive species generated during NTP treatment.

3.4 Conclusion

The non-thermal plasma efficiently inactivated spores with low energy consumption. The survival curve showed there were two phases in the inactivation process and majority of spore destruction occurred within the first three min reaching nearly complete sterilization. The survival curve, SEM images together with AFM images showed that spore surface was etched after NTP treatment and the two inactivation phases resulted from different plasma exposures in multiple spore layers. Water enhanced the spore destruction process as previously reported by generating hydroxyl radical or the vapor was working as an electric conductor. The etching may have been the result of oxidation caused by reactive species generated by plasma such as ozone. DPA was released and reacted with reactive species generated by plasma as indicated by the ATR-FTIR spectra.

Further research is needed to clarify what reactive species react with spore and how they cause the changes mentioned in our study.

CHAPTER IV
Characterization and Modeling of Bacterial Spore Germination Using FTIR and UV-Vis Spectroscopy

Abstract

Biochemical changes of spores during germination in different temperatures and after non-thermal plasma (NTP) treatment were monitored for up to an hour by combination of UV-Vis spectroscopy and attenuated total reflection Fourier-transform infrared spectroscopy (ATR-FTIR). The results showed that (1) bands of plasma treated spores increased more slowly and finally reached a lower level of absorbance compared with untreated ones; (2) large amount of DPA released in a short time when spores germinated in 50 ℃ showed that DPA released in response to heating; (3) the plot of fraction of germinated spore versus time indicates that the best temperature for spore germination is 30 ℃ with highest germination rate and proportion of germinated spores; (4) an empirical model based on Weibull distribution was established to describe spore germination process in order to better understand germination process. It showed that NTP treated spores could not follow the Weibull distribution because sub-lethal effects were induced by NTP and spore could not germinate normally.

4.1 Introduction

In last chapter, biochemical changes of spore after non-thermal plasma (NTP) treatment were studied. Plasma can induce dipicolinic acid (DPA) release and protein structure changes, and thus also has impacts on spore germination. In this chapter, spore germination and sub-lethal effects induced by non-thermal plasma (NTP) were studied.

During germination, DPA, which accounts for about 10% of the total spore weight [32], and its associated divalent cations Ca^{2+} are excreted from the core. The high core Ca-DPA level helps to reduce core water content, which is an important element in spore resistance to wet heat, and Ca-DPA also plays a more direct role in protecting spore DNA against several types of damage [18, 93, 94]. Due to the dehydrated state, the spore core has a high refractive index. As Ca-DPA releases in germination and replaced by water, the spore core's refractive index drops and light scattering by the spore core decreases significantly [95]. Finally, spore peptidoglycan degradation by activated cortex –lytic enzymes followed by swelling of the spore core with water further changes the spore refractivity, leading to a decrease of optical density at 600 nm (OD_{600}) [32, 95-98]. So the kinetics of spore germination can be measured by OD_{600} of spore cultures [32] and the fraction of germinated spores is linear related to the decrease in OD_{600} of the spore suspension [96]. However, the biochemical change of spores during germination was not reported by UV-Vis spectroscopy.

Attenuated total reflection Fourier-transform infrared spectroscopy (ATR-FTIR) is an easy and sensitive technique providing structural and chemical information at the molecular level. Some cellular components of bacteria can be identified by infrared spectroscopy [12], and constituents such as lipids, dipicolinic acid (DPA) and intracellular materials have been detected with this method [13]. The combination of UV-Vis spectroscopy and ATR-FTIR can provide more information about spore germination by linking fraction of germinated spores to specific molecular changes, especially DPA.

Few attempts have been made to model germination of bacterial spores. Germination model would contribute to understanding spore germination behavior under

different conditions and establish a rational framework for developing the food process for sterilization and for risk assessment that estimate the level of pathogen in a product at the point of consumption [99].

4.2 Materials & Methods

4.2.1 Spore preparation

The spore preparation protocol is the same as section 3.2.1.

4.2.2 Non-thermal plasma inactivation of spores

The non-thermal plasma (NTP) is generated by the dielectric barrier discharge (DBD), the same device as described in 3.2.3. BA spores water suspension (5μL and 10μL) was spread onto glass slide and waited until it dried in room temperature. The glass slide then placed in the plasma chamber at a distance of 2.6mm away paralleling to the upper dielectric barrier and receive NTP treatment for 1 min. Then the plate with 5μL spore suspension was washed by 1000 μL ST1 medium to a multiple reflection horizontal ATR (HATR) chamber to do ATR-FTIR analysis while the 10μL one was washed by 2000μL ST1 medium to a cuvette to do UV-Vis spectroscopy analysis at 23 ℃.

4.2.3 ATR-FTIR real time monitoring of spore germination

FTIR spectra were recorded using a FT-IR spectrometer (Excalibur 3100, Varian Inc. Palo Alto, CA) equipped with a liquid nitrogen cooled mercury cadmium telluride (MCT) detector. The sampling station was equipped with a Horizontal Attenuated Total Reflection (HATR) accessory with zinc selenide crystal (PIKE Technologies, Madison WI). The multiple reflection ATR spectrum only accounted for chemicals excreted by spores during germination because spore were not tightly in contact with ATR crystal. ST1 medium (1000 μL) was injected to the chamber of HATR accessory, and temperature was set to 23 ℃, 30 ℃, 40 ℃, 50 ℃ for each run respectively. After temperature was stable, 5μL spore suspension was loaded to the chamber. Multiple reflection spectra (12 reflections) of the samples were collected in the mid-IR region from 2000-1000 cm^{-1} (the fingerprinting region of microorganism) at a resolution of 4 cm^{-1} after averaging 32 scans at interval of 1 min. Data collection was stopped after 60 min.

4.2.4 Monitoring spore germination by UV-Vis spectroscopy

Spore suspension samples (10 μL) were thoroughly mixed with 2000 μL of ST1 medium preheated to 23, 30, 40, 50 ℃ in cuvettes for each run respectively. Cuvettes were put in the water bath in order to keep samples at the designated temperature. Cuvettes were taken out from water bath and optical density (OD) was recorded in every 2 min for up to 1 hour using UV-Vis spectroscopy.

4.2.5 Modeling of spores germination

The Weibull model was used in this study to describe the germination of spores according to previous studies [99, 100]. The germinated spore fraction can be quantified as the fraction decrease in OD_{600}. The form of Weibull function used was as follows:

$$S(t) = 1 - \frac{OD_t - OD_f}{OD_i - OD_f} = 1 - \exp\left[-\left(\frac{t}{\alpha}\right)^{\beta}\right] \quad \text{Equation 6}$$

where S(t) is germinated spore fraction at time t, OD_t is OD at time t, OD_i is initial OD, OD_f is OD of a fully germinated spore suspension, α is rate index, β is behavior index. Based on previous studies [101, 102], the parameter rate index α was modeled using an Arrhenius-type expression:

$$\ln(\alpha) = \ln(\alpha_{ref}) - \frac{E_a}{R} \times \frac{1}{T+273.15} \quad \text{Equation 7}$$

where α_{ref} is the scale parameter (min), Ea is the activation energy (kJ/mol), R is the ideal gas constant (8.314 J/mol/K), and T is the spore germination temperature (℃). Behavior index β is complex in the Weibull model because the spore germination process is a phenomenon involving multiple steps [100]. OD_f was recorded when the OD did not decrease any more. In this study, OD_f was determined by fully germinated spore suspension which was incubated in ST1 medium at 30 ℃ for about 5 hours, yielding a 14.34% reduction in OD. So OD_f equals 85.66% of OD_i was used for all samples in this study. The parameter estimation were performed by statistics software SPSS (IBM, Somers, NY).

4.2.6 Validation of model performance

The accuracy of model was assessed by the accuracy factor A_f and bias factor B_f [100, 103]. A_f indicates the spread of results about the prediction [103] and the modified form proposed by Baranyi et al. was used in this study [104]:

$$A_f = \mathrm{Exp}\left(\sqrt{\frac{\sum(\ln(\text{predicted value}) - \ln(\text{observed value}))^2}{n}}\right) \quad \text{Equation 8}$$

where n is the number of observations. B_f is a factor indicating whether a model, on average, over or under predicts the observed values or not [103]:

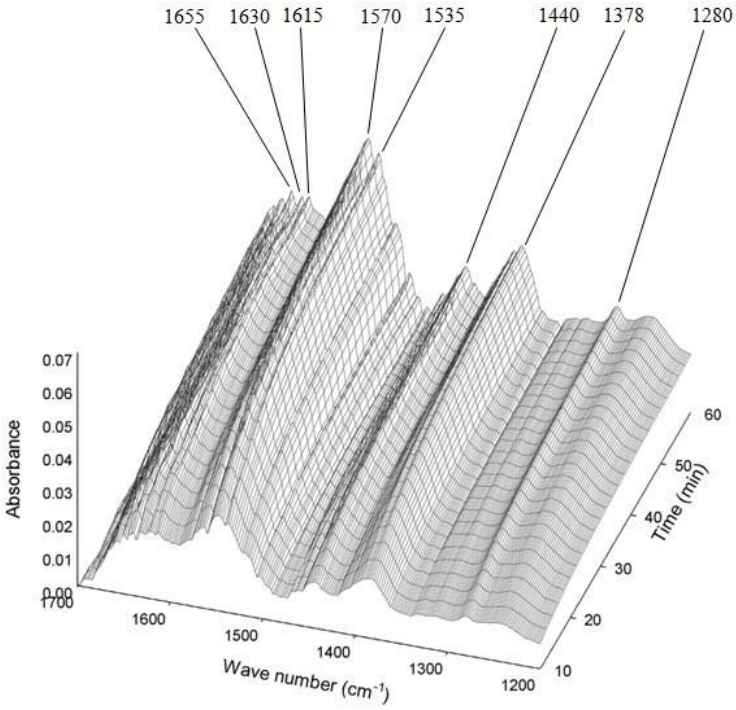
$$B_f = \mathrm{Exp}\left(\frac{\sum(\ln(\text{predicted value}) - \ln(\text{observed value}))}{n}\right) \quad \text{Equation 9}$$

4.3 Results and discussion

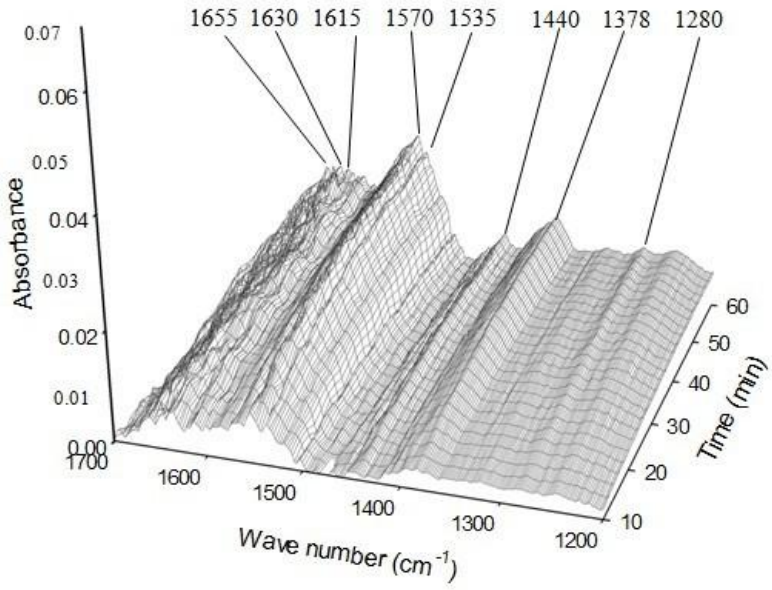
4.3.1 ATR-FTIR and UV-Vis spectroscopy analysis during spore germination at different temperatures

Figure 4-1A showed the dynamic changes in the multiple reflection ATR-FTIR spectra of germinating spores at 23 ℃ (Germination of NTP treated spores would be discussed in next section). Ca-DPA plays important roles in bacterial spore germination and is the most significant biomarker for *Bacillus* spores. Ca-DPA Mid-IR specific bands in *Bacillus* spores are at 1280, 1378, 1440, 1570, 1615 cm^{-1} (Table 3-2) and absorbances of these bands are correlated to the DPA released by spores during germination. Band at 1570 cm^{-1} that correlated to C-N vibrations of the DPA ring [79] was chosen for probing the release of DPA because it had the most

intensive signal and the signal only accounts for the specific DPA ring structure. As shown in Figure 4-1A, the intensities of DPA were increasing as time went on.



(A)



(B)

Figure 4- 1 Three-dimensional spectra of germinating spores (A) control at 23 ℃; (B) plasma treated spores at 23℃.

Figure 4-2 shows the absorbance of the 1570 cm^{-1} band change which corresponds to Ca-DPA during spore germination and the increase of absorbance indicated release of DPA. At 23, 30 and 40 ℃, DPA released quickly at the beginning and then slowed down. Finally the absorbance tended to be stable showing that spores released DPA at a very slow rate. As for spores germinated at 50 ℃, the absorbance of DPA increased dramatically from 4 min to 8 min, and then slowed down but still increased more quickly than it did at 23, 30 and 40 ℃. It was possible that unnatural release occurred due to heat. The final recorded absorbance of 1570 cm^{-1} band of spores grown at 50 ℃ was more than twice spores grown at 23, 30 and 40 ℃.

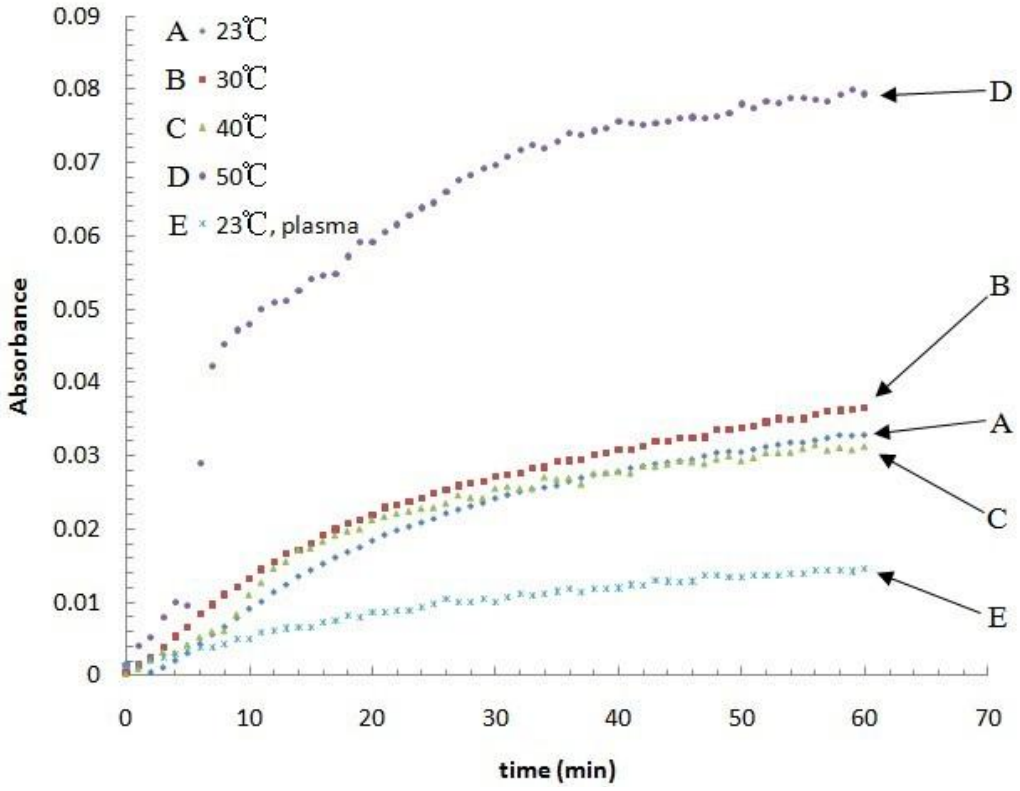


Figure 4- 2 Absorbance of the Ca-DPA specific IR band at 1570 cm^{-1} as a function of time in spore germination: (A) 23 ℃; (B) 30 ℃; (C) 40 ℃; (D) 50 ℃; (E) 23 ℃, plasma treated.

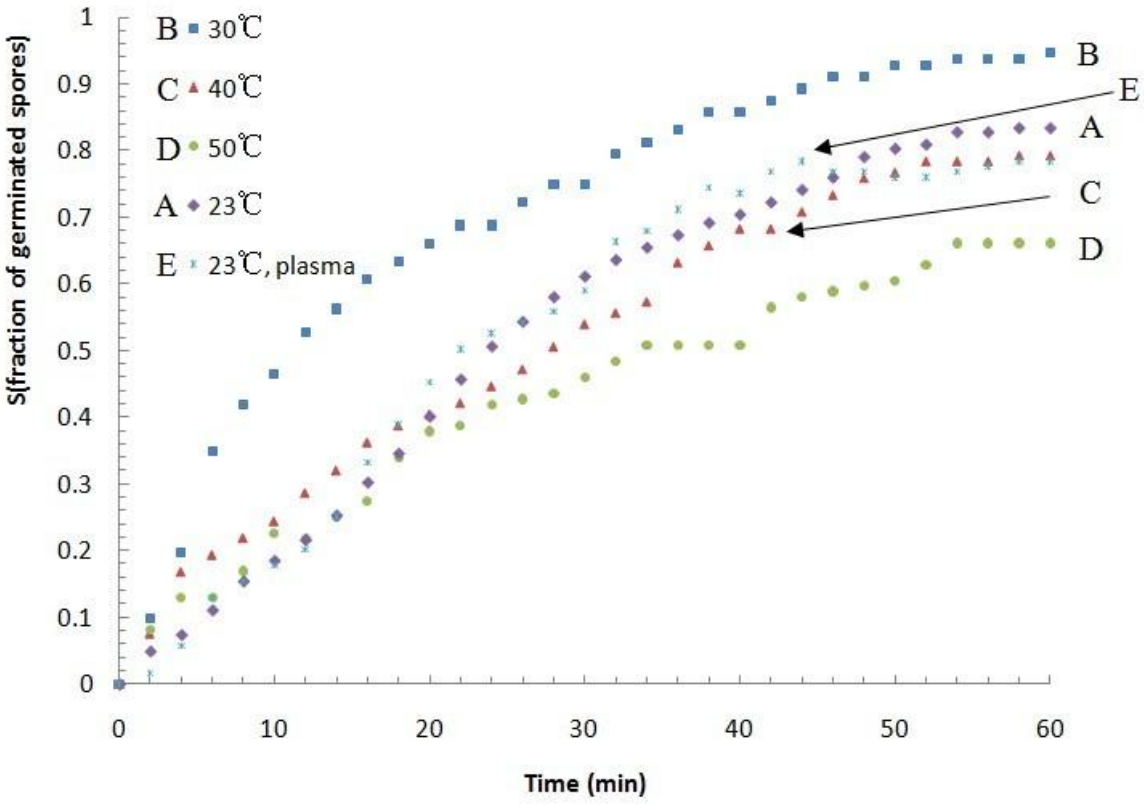


Figure 4- 3 Germination curve of spores germinated in (A) 23 ℃, (B) 30 ℃, (C) 40 ℃, (D) 50 ℃, (E) Plasma treated at 23 ℃ as measured by OD_{600}.

Figure 4-3 is the germination curve showing that the fraction of germinated spores as a function of time determined by UV-Vis spectroscopy according to the refractivity changes during spore germination. The curves of spores germinated under different temperatures were similar in that spores grew faster at the beginning and then slowed down. Spores at 30 ℃ had the largest fraction of germinated spores, as high as 94.6%, followed by 23 ℃ with 83.3% germinated spores; while spores in relatively high temperature conditions at 40 and 50 ℃, had fewer germinated spores with only 79.2% and 66.1% respectively.

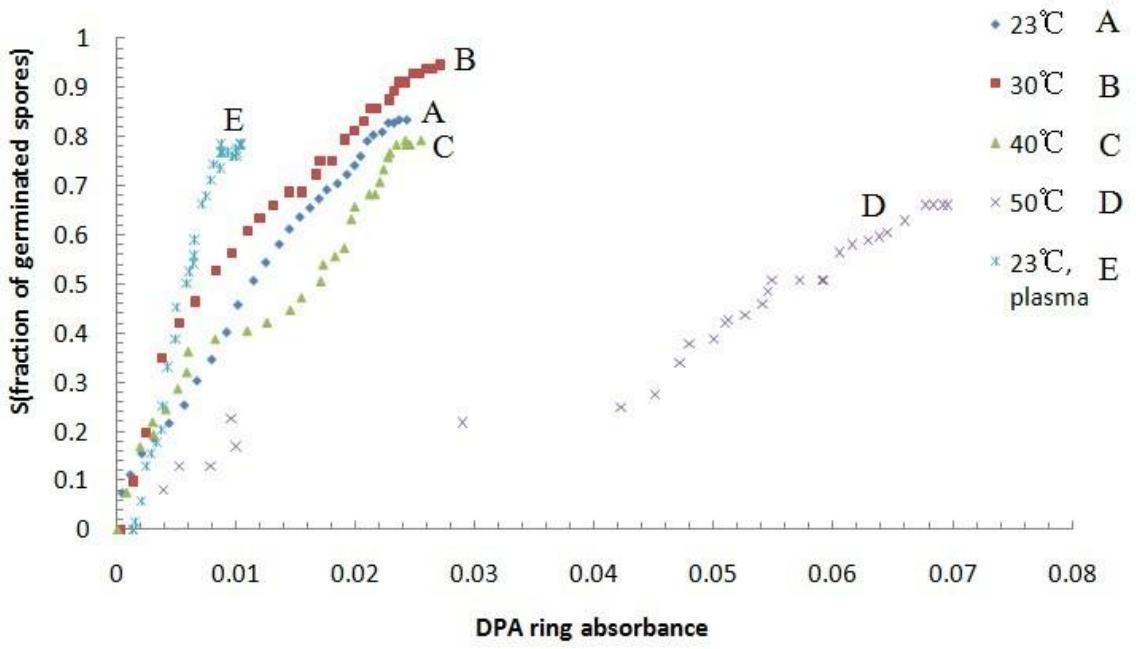


Figure 4- 4 The fraction of germinated spores versus absorbance of the Ca-DPA specific band at 1570 cm^{-1}

Spores under all temperatures could germinate, even though at 50 ℃ spores released a greater amount of DPA.

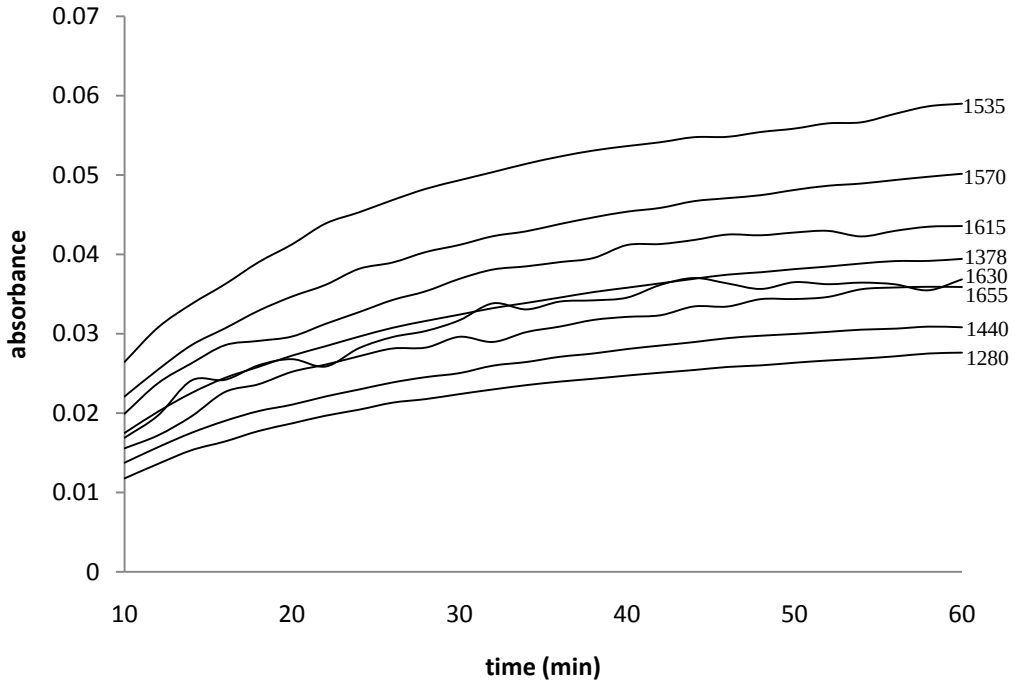
Figure 4-4 shows a plot of the fraction of germinated spores versus the absorbance of the Ca-DPA specific band at 1570 cm^{-1}. Plots of 23 and 30 ℃ indicate that a correlation between the amount of Ca-DPA released and the fraction of germinated spores. As for spores at 40 ℃ and 50 ℃, there was a plateau phase indicating that DPA released quickly while the fraction of germination did not change significantly

4.3.2 Germination of spores after sub-lethal NTP treatment

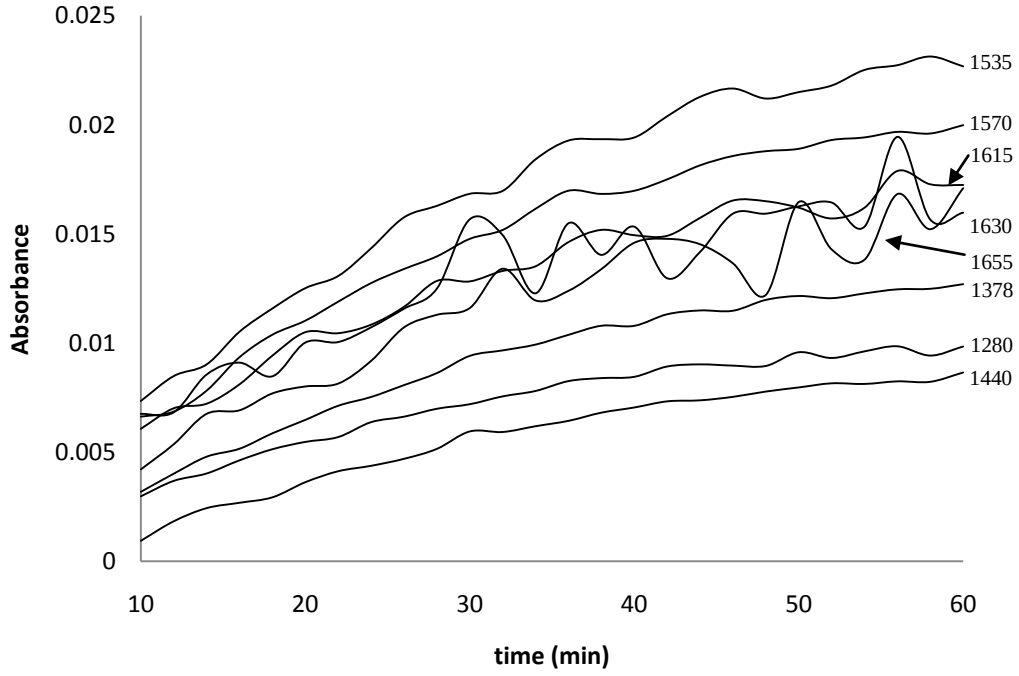
Figure 4-1B shows the dynamic changes in the ATR-FTIR spectra of spores received 1 min NTP treatment during germination at 23 ℃. Compared with the control one, although intensities of DPA bands also increased in plasma treated spores, the increasing rate is much slower and the absorbance ended up much smaller than the control ones, as it was also indicated in Figure 4-5.

ATR-FTIR was able to capture the subtle biochemical and structural changes that occurred during germination and the curve of each band followed the expected pattern of DPA release and protein synthesis at the initiation of spore germination (Figure 4-5). As spores became actively growing bacteria, the absorbance increase of DPA and protein structure bands diminished.

The germination of plasma treated spores exhibited a similar spectral pattern (Figure 4-5) as untreated control spores. However, some differences were also observed. The absorbance of bands from plasma treated spores was much lower than the controls likely due to the initially lower spore abundance in the plasma treated samples. However the possibility that plasma treated spores exhibit abnormal function of DPA release and protein synthesis cannot be excluded based solely on the data presented. Curves of 1630 cm^{-1} and 1655 cm^{-1} bands absorbance that correspond to protein structure wiggle compared with the control, indicating that these bands shifted and these protein structures changed. It is also possible that polypeptide structure changed as the 1535 cm^{-1} band wiggles too. The proteins synthesized by spores after NTP treatment might be malfunction.



(A)



(B)

Figure 4- 5 Absorbance at significant wavelengths at different time: (A) control; (B) plasma treated spores

Figure 4-3 shows that the plasma treated spores have a similar germination curve with the untreated one. However, the fraction of germinated spores at 60 min was 78.4%, which was not as much as spores germinated at 23 and 30 ℃.

In Figure 4-4, the plasma treated spores shows a linear relationship between the amount of Ca-DPA released and the fraction of germinated spores but with a larger slope, indicating that small amount of DPA release was detected during germination because DPA was reacted with reactive species generated by NTP, but they could grow to some extent.

4.3.3 Modeling of spore germination

The effect of temperature and NTP treatment on spore germination was examined by fitting the Weibull function to the germination curve. The Weibull function parameters estimates are shown in Table 4-1. At all temperature levels, the Weibull function described the germination data well, giving R^2 above 0.99. The plasma treated R^2 (0.978) is slightly smaller, indicating non-thermal plasma interferes with the natural growth of spores. The rate index α increased as the fraction of germination decreased, such that model for spores germinated at 30 ℃ had the smallest rate index α while the 50 ℃ model had the largest value. It is possible that lower index α indicates faster germination. The behavior index β is irregular considering that the spore germination process involved multiple steps [100].

Table 4-1The Weibull model parameters rate index (α) and behavior index (β) at different temperatures

T, ℃	α	β	R^2
23	33.748 ±0.675 *	1.231 ±0.054	0.995
30	18.128 ±0.56	0.866 ±0.040	0.995
40	36.783 ±1.094	0.989 ±0.057	0.990
50	52.932 ±1.639	0.857 ±0.041	0.993
23, plasma treated	33.442 ±1.467	1.147 ±0.106	0.978

* 95% confidence interval

Table 4-2 Empirical model accuracy (A_f) and bias factors (B_f) for the spore germination in different temperatures

T, ℃	A_f	B_f
23	1.105	0.993
30	1.078	1.010
40	1.125	0.970
50	1.088	0.990
23, plasma treated	**1.216**	1.063

* In this study, $A_f \leq 1.15$ was considered good; B_f values in the 0.91 to 1.05 range were considered good.

In evaluating the model involving pathogens, B_f values in the range of 0.90-1.05 can be considered good, 0.7-0.9 and 1.06-1.15 are considered acceptable [100, 103]. In this study, the B_f value of the NTP treatment (1.063) slightly exceeded 1.05, but the B_f values of the untreated spore were in the range of 0.90-1.05 as shown in Table 4-2. With A_f value equals to 1 indicating perfect consistency between predicted and observed values [105], an increase of 0.1-0.15 for every variable in the model can be considered good [100] and time is only variable included in this model. So $A_f \leq 1.15$ was considered good in this study and despite the A_f value of plasma treated one is larger than 1.15, the model of untreated ones are good. Figure 4-6 shows the Weibull model fit the data very well indicating that Weibull model is suitable for modeling spore germination except NTP treated spores because they exhibited different germination pattern.

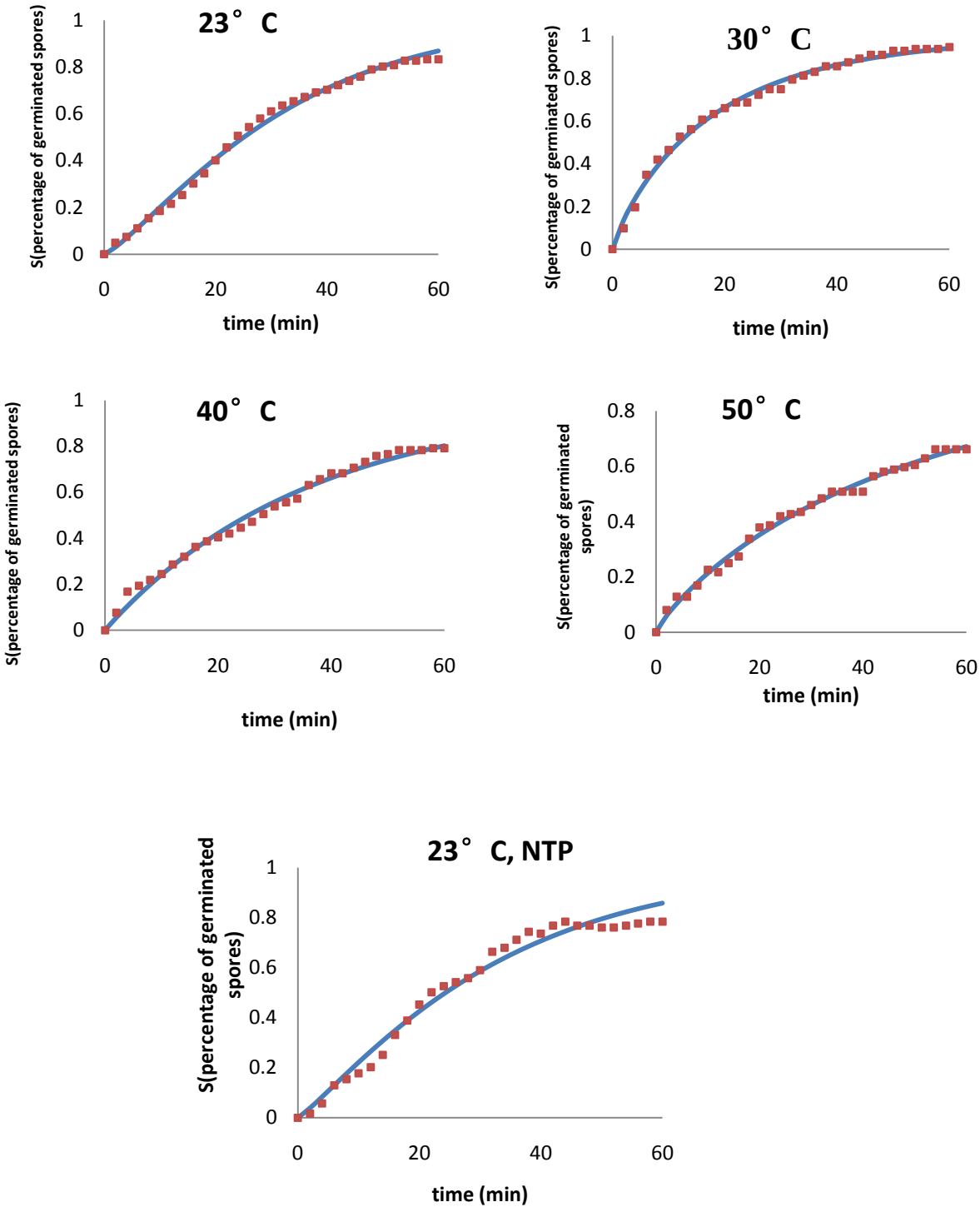


Figure 4- 6 Scatter plot of fraction of germinated spores (S) and Weibull model predicted line of S over time.

4.4 Conclusion

Spores undergo biochemical changes during germination as indicated by the increasing absorbance of IR bands. Though the bands of NTP treated spores also increased, the increasing rate was slower and the reached a lower level of absorbance compared with the untreated, which indicates the plasma induces sub-lethal hazard to spores.

Large amount of DPA released in a short time when spores germinated in 50 ℃ indicates that DPA would release in response to the heat, which is in agreement with previous studies [12, 13, 94]. Spores with higher Ca-DPA level may have higher moist heat resistance since they have lower core water levels. This study may be useful for analysis of the spore moist heat resistance during sterilization process.

The germination curve indicates that the best temperature for spore germination is 30 ℃ as in this condition the germination rate is the largest. This may be contributed to the combined heat and high pressure sterilization process since vegetative cells are easier to kill than spores. In other words, spores can be induced to germinate and then sterilized. Heat will suppress the spore germination and the plasma induced sub-lethal hazard to spores as indicated by FTIR spectra as indicated by a lower fraction of germinated spores

A correlation between the rapid drop in spore refractivity indicated by the UV-Vis spectroscopy and complete of Ca-DPA release was observed when spores germinated in 23 and 30 ℃. Previous study[95] also has similar conclusion. However, due to the large amount of Ca-DPA release when spores in high temperature, the correlation cannot be

established in spore germinating in high temperature. Further studies are needed to investigate the mechanism of Ca-DPA release in high temperature.

An empirical model based on Weibull function successfully described the germination data at all level of temperatures. The rate index α increased as the germination rate decreased. However, this model did not fit the germination data of plasma treated spores, which indicated that germination of plasma treated spore was different from untreated ones. Given the correspondence between spore refractivity and Ca-DPA release in mild condition together with the empirical model, a relationship between fraction of germinated spores and amount of Ca-DPA release can be established in order to further reveal the mechanism of spore germination.

CHAPTER V
Comparison of Mechanisms of Inactivation of *Bacillus amyloliquefaciens* Spores Using FTIR

Abstract

Thermal and chemical methods are frequently used to inactivate bacterial spores. A close investigation of these techniques in comparison to the non-thermal technology of high pressure processing and non-thermal plasma (NTP) is important to better understand the different mechanisms of inactivation by these techniques and to gain more efficient control of spores. This study is aimed at using Fourier-transfer infrared spectroscopy (FTIR) technique to investigate the effects of these different inactivation treatments on *Bacillus amyloliquefaciens* (BA) spores, a ubiquitous bacterial strain in soil and popular for use in foods as a pressure-surrogate to *Clostridium botulinum*. High-pressure (80 kpsi at 65 ℃), autoclaving (121 ℃ for 15 min), and chemical treatment using aqueous chlorine dioxide (CD) solution (100-220 ppm for > 1 h) were compared with NTP. Besides, two different feed gas, air and argon, were used in NTP and compared. Treated spores together with the untreated control were examined for their different morphological and biochemical changes in response to these inactivation treatments. Results showed that autoclave and high pressure inactivated spores by mechanic force as no changes in DPA peaks; while chemical treatment and NTP with air as feed gas treatment inactivated spores by oxidation. Chlorine dioxide might oxidize DPA and carboxylate was generated. DPA was released during NTP with argon as feed gas treatment, and UV emission or charged particle might accounts for the inactivation. This

methodology will provide a useful new tool to rapidly examine bacterial spores after different sporicidal treatments.

5.1 Introduction

Bacterial sterilization is an important process in food engineering. Several techniques have been developed in the past. These include autoclaving as the most common heat treatment, while chlorine dioxide (CD) is a common chemical used to inactivate bacteria. However, both of these techniques have restrictions in their application to the food industry: CD treatment results in unpleasant taste and odor, and the heat generated during autoclaving causes the loss of nutrients, neither of which is desirable in food processing. In recent years, new non-thermal technique, namely high-pressure and non-thermal plasma (NTP) treatments, show substantial promise in food processing, due to its sterilization ability without heating the sample. To date, few attempts have been made at a close comparison of the inactivation results among the mechanisms of these inactivation techniques at the morphological and chemical levels.

This study was undertaken to investigate the effects of five different microbial inactivation treatments (chlorine dioxide, autoclaving, high-pressure and non-thermal plasma using air or argon as feed gas), and used *Bacillus amyloliquefaciens* (BA) spores as model microorganism because they are resistant to unfavorable conditions and surrogates of *Clostridium Botulinum* in food processing and anthrax which was used to produce bio-warfare.

5.2 Materials & Methods

5.2.1 Spore preparation

The spore preparation protocol is the same as that described in section 3.2.1.

Chemical treated (the solution containing 100-200 ppm chlorine dioxide was used as the chemical treatment, treatment time was more than one hour), autoclaved (14.84 psi gauge pressure and 121^{o} C for 15 minutes), high pressure (high-pressure treatment was 80,000 psi at 65^{o} C for 2 hours) treated and control samples were centrifuged at 5000 rpm for 5 min in order to isolate the spore pellets. The deposited spores were rinsed with sterile distilled water, again centrifuged, and re-suspended with distilled water. These rinsing steps were repeated three times to remove the residual chemicals. The clean BA suspension was freeze-dried for 12 hours using LABONCO Freezone 4.5 at -47 ℃ and 1.653×10^{-3} psi and spore powders were collected. The NTP generation using air as feed gas was the same as described in section 3.2.2. NTP using argon as feed gas was operated in a sealed chamber with an inlet and an outlet for argon gas flow with a flow rate of 60 mL/min. Spores were treated for 3 min by NTP (air or argon as feed gas) as described in section 3.2.3. After treatments, spores were scraped from the glass slide and spore powders were collected.

5.2.2 Morphology study by Scanning Electron Microscope

Spore powders were diluted with sterile distilled water and spread on the silicon specimen chip supports attached to the scanning electron microscopy (SEM) pins via

copper tape. As for the non-thermal plasma (NTP) treatments, the devise set up was the same as described in section 3.2.2 and the flow rate of argon is 100 mL/min. Spores were NTP treated using air or argon as feed gas for 3 min on silicon chip specimen supports which directly attached to the scanning electron microscopy (SEM) pins. After spores dried at room temperature, samples prepared along with untreated control were coated with gold by vacuum evaporation prior to SEM (Zeiss 1525, Carl Zeiss SMT Inc.) observation.

5.2.3 Morphology study by Transmission Electron Microscopy

Autoclave, high pressure, chemical treated and control BA samples were kept in fixative solution (3% Gultaraldehde in 0.1M cacodylate) at room temperature for an hour, and then rinsed with 0.1 M sodium cacodylate buffer (pH 7.2) for 10 min 3 times. The samples were post-fixed with 2% OsO_4 in 0.1M cacodylate buffer at room temperature for 1 hour. The post-fixed samples were then dehydrated through a sequential treatment of ethanol solution with increasing concentration: 25%, 50%, 70%, 95% and 100% for 15 min, respectively, and also treated with 100% acetone for 15 min twice. The samples then were dehydrated in 2:1 EtOH/Spurr mixture for 1 hour, then in 1:2 EtOH/Spurr mixture for 12 hours, and finally in 100% Spurr for 4 hours. The sample was transferred into embedding molds with complete Spurr mix, and polymerization was carried out in an oven at 68℃ for 24 hours. Upon the completion of the procedures above, the specimens were observed by transmission electron microscopy (TEM) (Hitachi H-800, Nissei Sanqyo America, LTD.).

5.2.4 Fourier transform infrared spectroscopy analysis

Fourier transform infrared (FTIR) spectra were recorded using a FT-IR spectrometer (Excalibur 3100, Varian Inc. Palo Alto, CA) equipped with a liquid nitrogen cooled mercury cadmium telluride (MCT) detector. The sampling station was equipped with an overhead Attenuated Total Reflection (ATR) accessory with germanium crystal (PIKE Technologies, Madison WI). The spore powders of autoclave, high pressure and chemical treated and NTP (air or argon as feed gas) treated samples were placed on the KBr plate for each sampling. Each FTIR spectrum was collected in the mid-IR region from 1800 to 1200 cm^{-1}, which is the fingerprint region of bacterial spores, at a resolution of 4 cm^{-1} after averaging 128 scans to improve the signal-to-noise ratio. Single reflection spectra of the samples were obtained and presented in absorbance units after taking into account the background spectrum of air. The ATR crystal was carefully cleaned with ethanol and dried between successive measurements to prevent cross contamination. There are 20 spectra of high pressure treatments, 22 of untreated control, 24 of chemical treatment, 8 of autoclave, 15 of NTP with air as feed gas and 20 of NTP with argon as feed gas.

5.3 Results and Discussion

5.3.1 Morphology study by scanning electron microscope

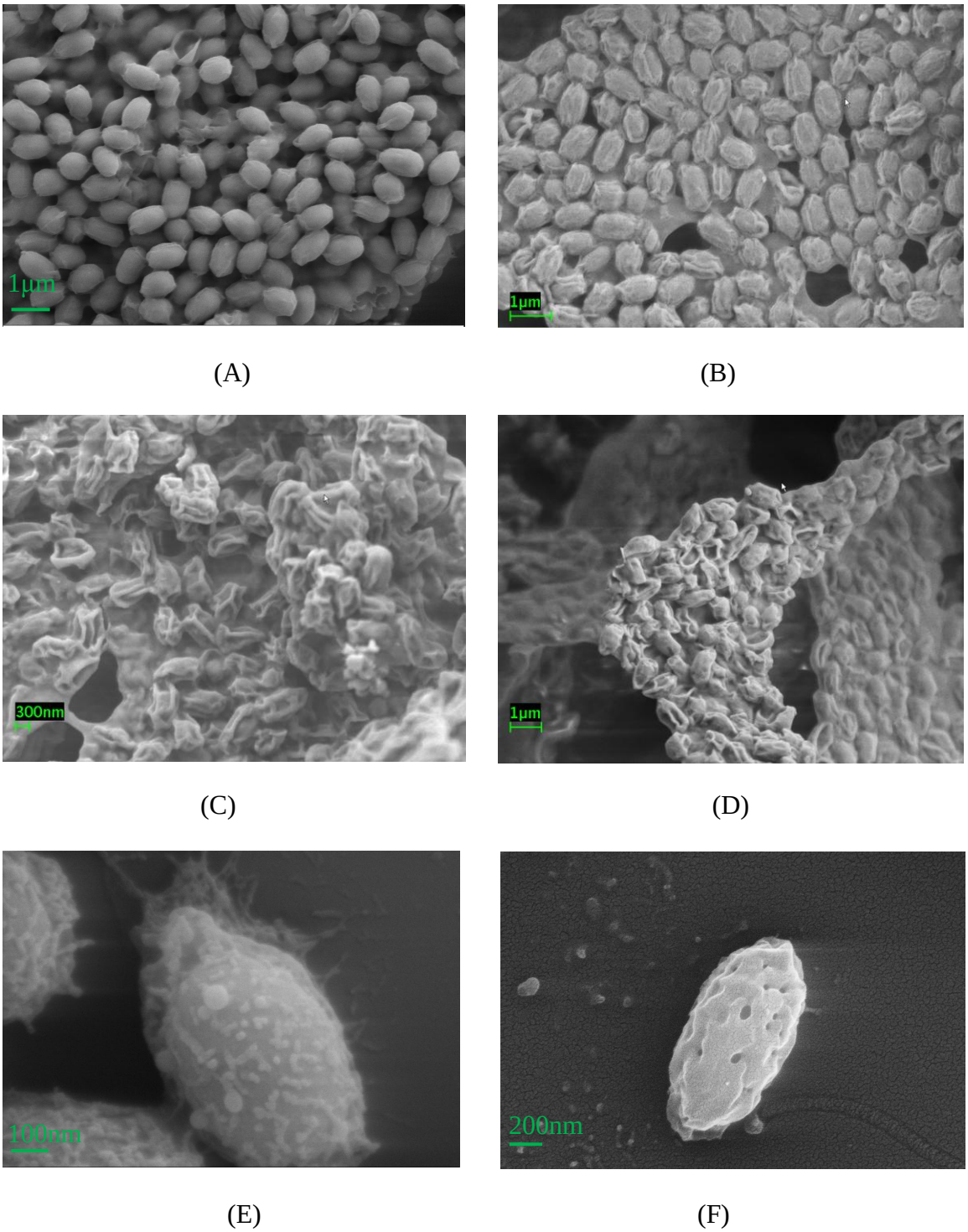


Figure 5- 1 SEM image of dried BA samples: (A) control; (B) chemical (CD) treated; (C) autoclaved; (D) high-pressure treated; (E) NTP using air as feed gas and (F) NTP using argon as feed gas treated.

Figure 5-1 shows SEM images of control spores and spores after chlorine dioxide (CD), autoclave, high pressure and non-thermal plasma (NTP) using air or argon as feed gas treatments. The control BA spores were in the intact oval shape with smoother surfaces, as compared to the treated spores. CD treatment caused little morphological change but spore surfaces were oxidized and wrinkled slightly. Both autoclaving and high-pressure treatments caused significant morphological damage, as the spores look like being squeezed. NTP using air as feed gas treated spores showed a similar pattern with CD treated one, with the spore surfaces etched away randomly and no indication that mechanic force applied on spore surfaces. Spores treated by NTP using argon as feed gas exhibited different pattern that only few holes observed on spore surface.

SEM images showed that it was possible that mechanical forces were the essential cause for the spore inactivation by autoclaving and high-pressure treatments. Cellular components were released upon application of the external mechanical forces. CD treatment took a completely different path, which probably broke up the cell by oxidization. NTP with air as feed gas treated spores might react with the reactive species such as ozone and other oxidants. NTP using argon as feed gas would not generate any reactive species, so the UV emission and charged particle might accounts for the inactivation.

5.3.2 Observation by transmission electron microscopy

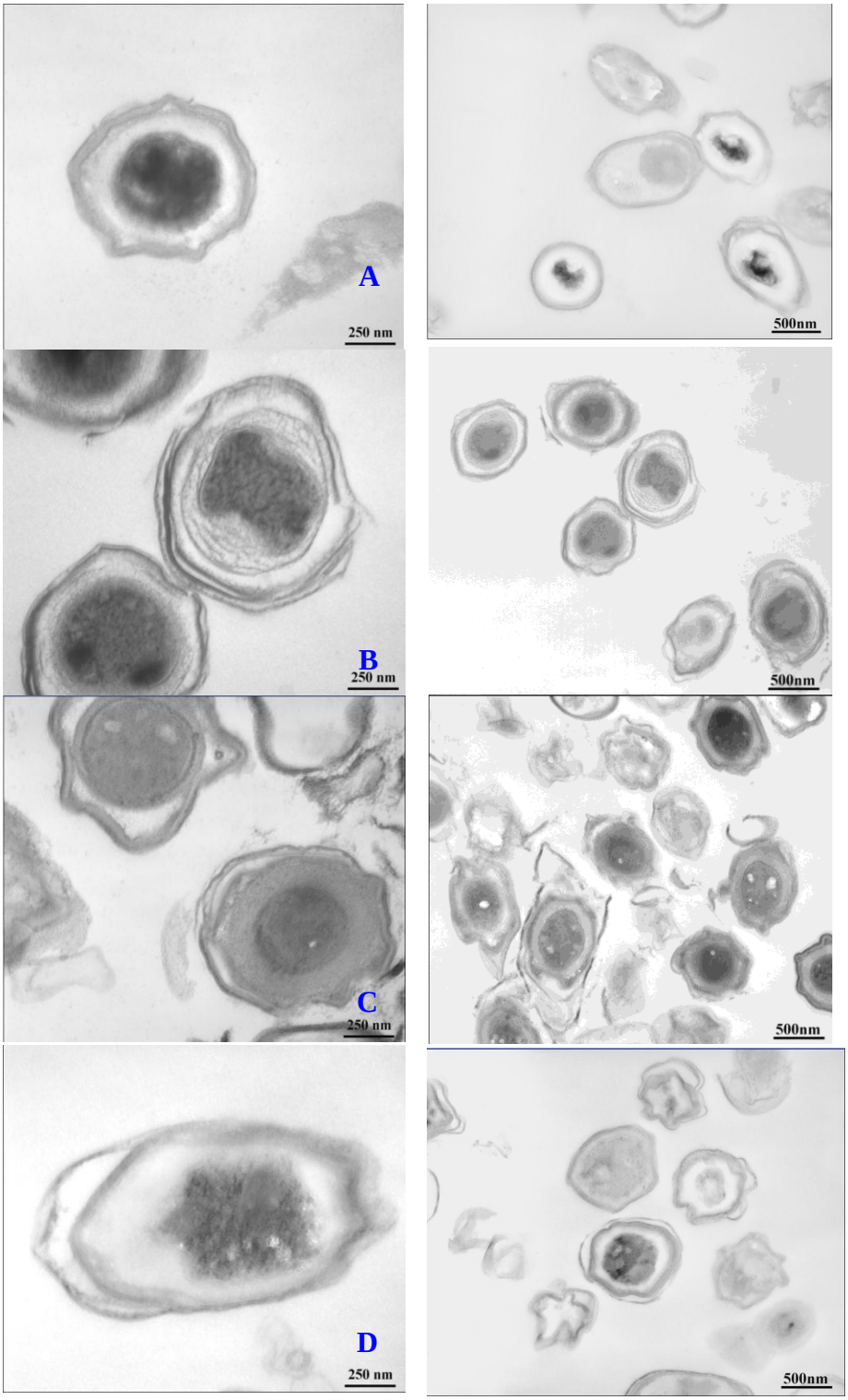


Figure 5- 2Transmission electron microscopic images of the fixed BA samples: (A) control; (B) chemical treated (CD); (C) autoclaved; (D) high pressure treated; and (E) non-thermal plasma treated with 20,000 magnification (left column) and 10,000 magnification (right)

Figure 5-2 shows TEM images of the control BA samples (A), CD treated (B), autoclaved (C), and high-pressure treated samples (D). CD treatment had little change of the spore morphology. However, some additional substances were observed within the cortex and the core was not as dark as the control spores for the chemical treated spores. Again, it was clear that the spore morphology was changed significantly by the autoclaving treatment, and the outer membrane exhibited an irregular contour. Furthermore, the cortex was dark and looked like filled with substances excrete from the spore core. As for the high pressure treatment, the contour of spore core was irregular and the spore looked like burst.

5.3.3 Fourier transform infrared spectroscopy analysis

Figure 5-3 shows the FTIR spectra of control spores and spores after autoclave, CD, pressure, NTP with air or argon as feed gas treatments. Spectra of autoclave, high pressure and NTP with argon as feed gas treated spores had larger absorbance compared with the control. However, spectra of CD treated spores had lower absorbance especially between 1492 cm^{-1} and 1566 cm^{-1} and the shape changed. Also the spectra of NTP with air as feed gas treated spores had the lowest absorbance. It is possible that autoclave and high pressure treatment inactivated spores by mechanic force and cell components were squeezed out, while cell components of spores after NTP with argon as feed gas treatment released so that spectra had higher signal. And CD oxidized some cell components so that changed the shape and absorbance of the spectra. As for NTP with air as feed gas treated spores, our previous research indicated DPA was released in response to plasma and then reacted with reactive species such as ozone.

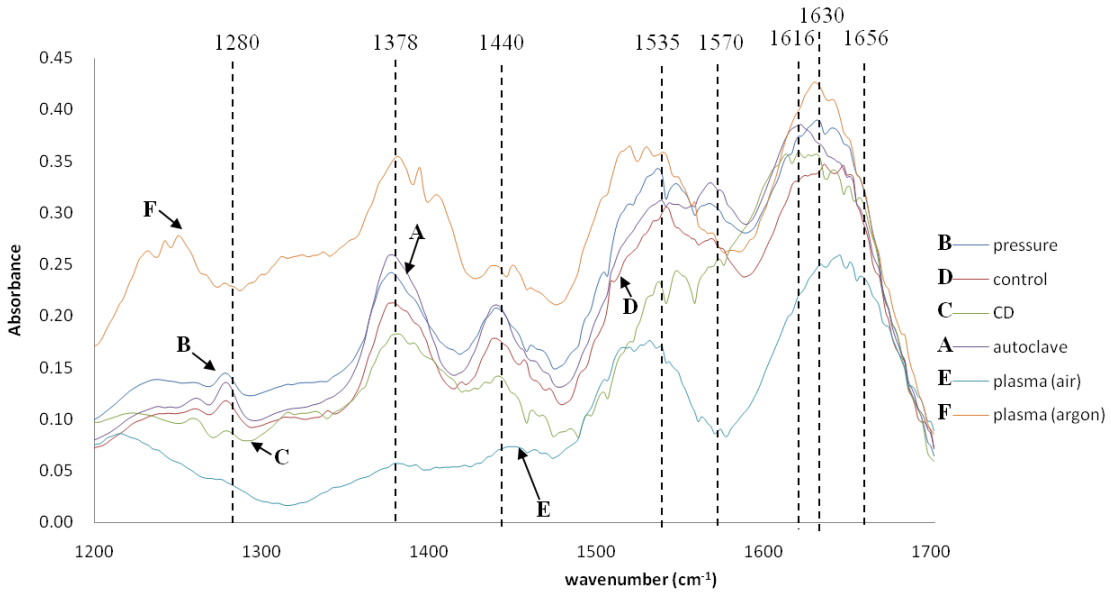


Figure 5- 3 FT-IR spectra of control spores and spores after (A) autoclave, (B) pressure, (C) chemical treated (CD), (D) control, (E) NTP with air as feed gas, (F) NTP with argon as feed gas treatments.

Peaks of spectra were not sharp enough and it was difficult to pick up peaks that had significant change after inactivation treatments and made a fair comparison difficult only based on spectra. In this study, principal component analysis (PCA) and soft independent modeling of class analogy (SIMCA) were employed to analyze the spectra. Figure 5-4 shows the three dimension score plot of all samples in PC1, PC2 and PC3. The CD and plasma treated spores were easy to separate from the others. However, control spores and spores after autoclave and high pressure treatments could not be separated, indicating there are few chemical changes of spores in autoclave and high pressure treatments.

First, spectra of control spores and spores after CD and NTP with air or argon as feed gas treatments were studied by SIMCA approach. The discriminating power of a variable gave information about its ability to discriminate between any two models.

Discrimination power plot can be used to identify the spectral wavenumber and associated functional groups that had significant differences in SIMCA class projections. Higher value of discrimination power indicates greater influence of that wavenumber in classifying the samples which means greater differences.

Principle component analysis (PCA) is used to decompose the data into new principal component coordinate space in order to better reveal the data structure. The principal component (PC) is the direction (axis) that has the maximum variance [106] and first principal component (PC1) has maximum variance, followed by second, third and so on. A score vector is the vector from all objects projected down onto one particular principal component [106]. Scores are the coordinates of samples in new principal components. The score plot can be used to identify groups. Loadings are the correlation coefficients between variables and principal components. Loading plot of a certain principal component is useful for the assignment of diagnostic spectral bands.

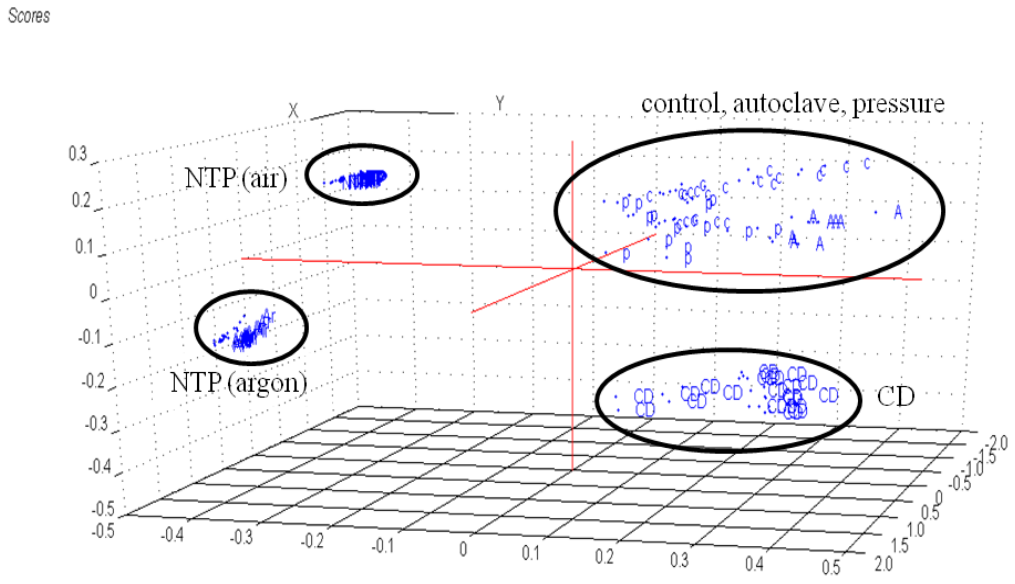
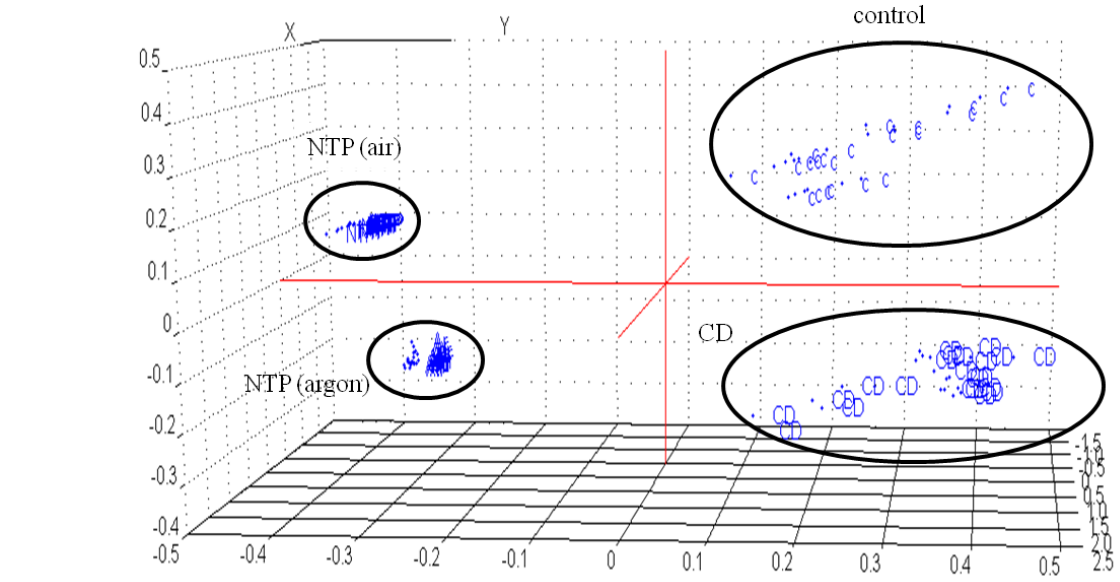
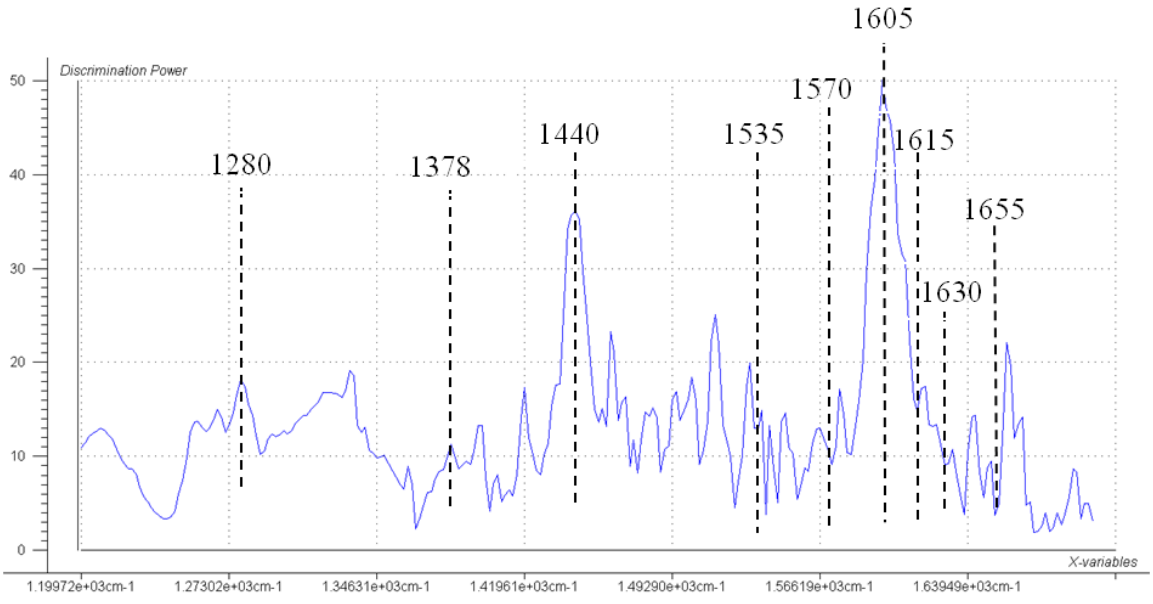


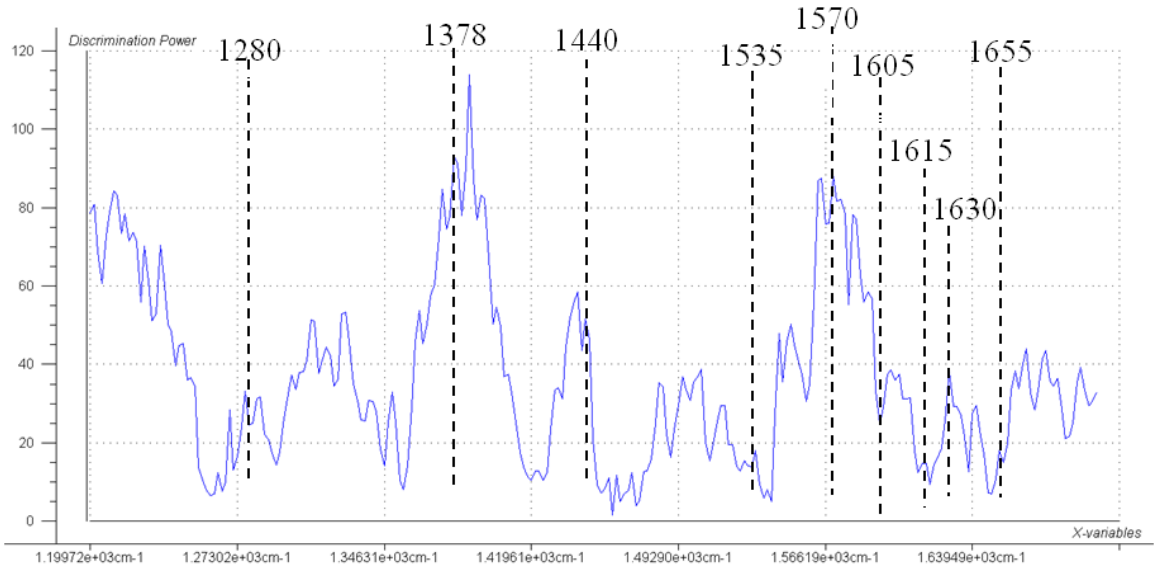
Figure 5- 4Score plot of all samples in PC1, PC2 and PC3: Control (C), Autoclave (A), chlorine dioxide (CD), High pressure (P), Non-thermal plasma (NTP).



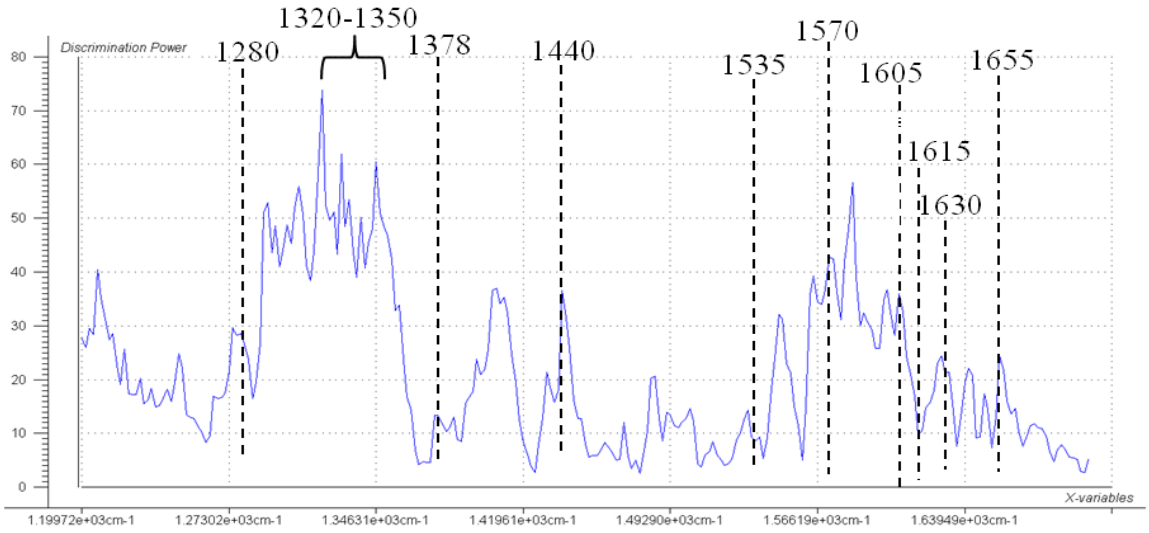
(A) Score plot of control and spores after CD and NTP treatments (air or argon as feed gas)



(B) Discrimination power plot of control VS CD treatment



(C) Discrimination power plot of control VS NTP (air) treatment

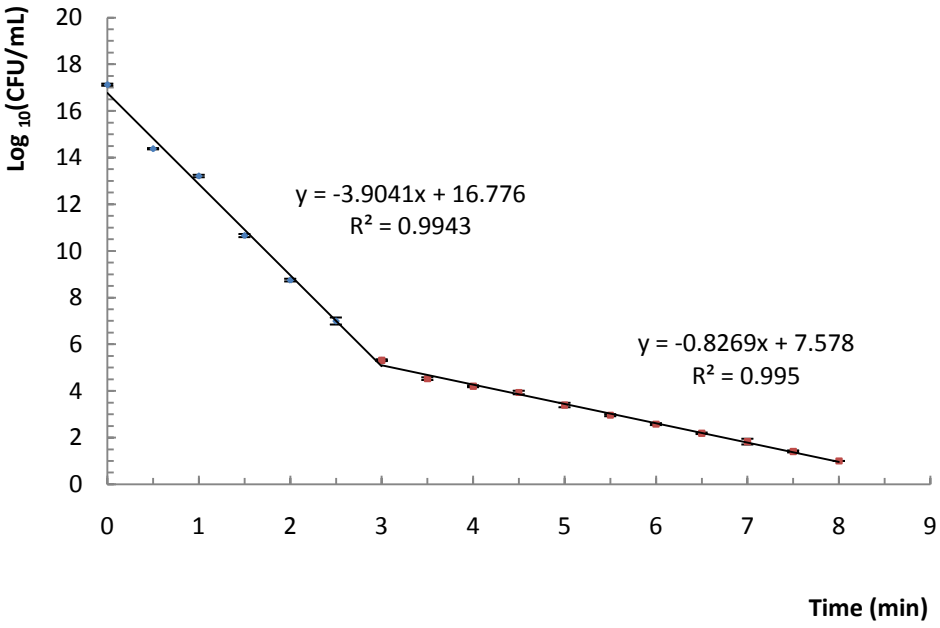


(D) Discrimination power plot of control VS NTP (argon) treatment

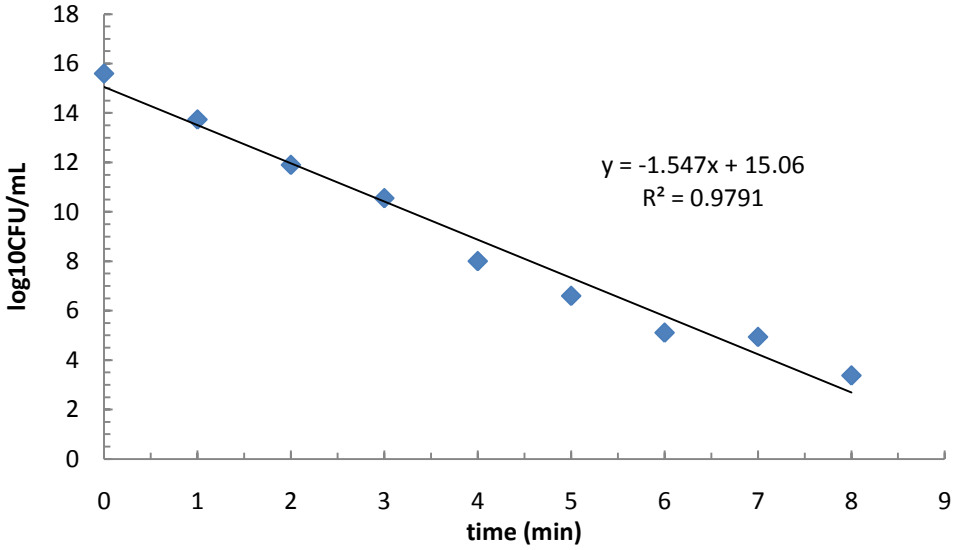
Figure 5- 5 SIMCA analysis of control and spores after Chemical (CD) and NTP (air or argon as feed gas) treatments

Figure 5-5A shows the SIMCA class projection plot that visualize the sample clusters on the three PC axes and all the four distinct clusters which were differed from treatment type were well separated in 3D space. Figure 5-5B shows the discrimination power plot of control vs. CD treated spores, Figure 5-5C shows the discrimination power

plot of control vs. NTP with air as feed gas treated spores and Figure 5-5D shows the discrimination power plot of control vs. NTP with argon as feed gas treated spores. The IR band in 1605 cm^{-1} is the symmetrical carboxylate stretching vibrational band whose intense increased significantly after CD treatment as discrimination power was high and in original spectrum this band of CD treatment was larger than control. It indicated that CD oxidized the spore and generates carboxylate. The discrimination power of IR band for acid peptides and DPA pyridine ring vibration in 1440 cm^{-1} was also significant in CD treatment and the absorbance decreased after treatment. It indicates CD might also oxidized acid peptides and DPA. As for the discrimination plot for NTP with air as feed gas treatment, IR bands of 1378 cm^{-1} (the stretching bands of COO- groups of dipicolinic acid (DPA)-Ca chelate [12]) and 1570 cm^{-1} (C-N vibrations of the DPA ring bands) decreased significantly as discriminating power was large and in original spectrum this band of CD treatment was smaller than control; the absorbance of 1280 cm^{-1} band (DPA and amide III band of proteins), 1440 cm^{-1} band (DPA pyridine ring vibration [88, 89] and acid peptides [81]) also decreased. The decreasing of DPA bands indicated the DPA released and reacted with reactive species. CD treatment had low discrimination power in both 1630 cm^{-1} band and 1655 cm^{-1} band, while NTP with air as feed gas treatment had relatively high discrimination power, which indicates NTP using air as feed gas had more impacts in destroying the secondary protein structure. IR absorbance of spores after NTP with argon as feed gas treatment increased compared with control. And discrimination power of IR bands in 1320~1350 cm^{-1} (C-N stretch), 1570 cm^{-1} (C-N vibrations of the DPA ring bands) and 1440 cm^{-1} (acid peptides and DPA pyridine ring vibration) were large, indicating DPA released during inactivation.



(A)



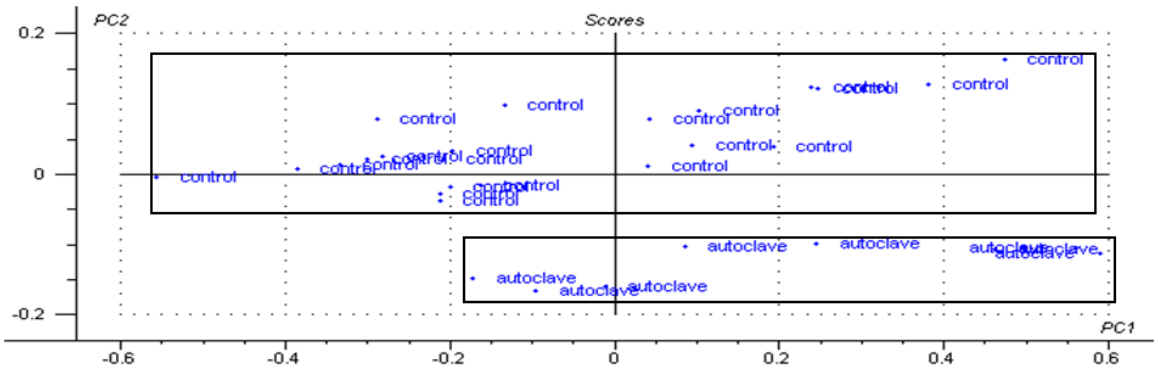
(B)

Figure 5- 6 Survival curve of (A) NTP (air), (B) NTP (argon) inactivation process

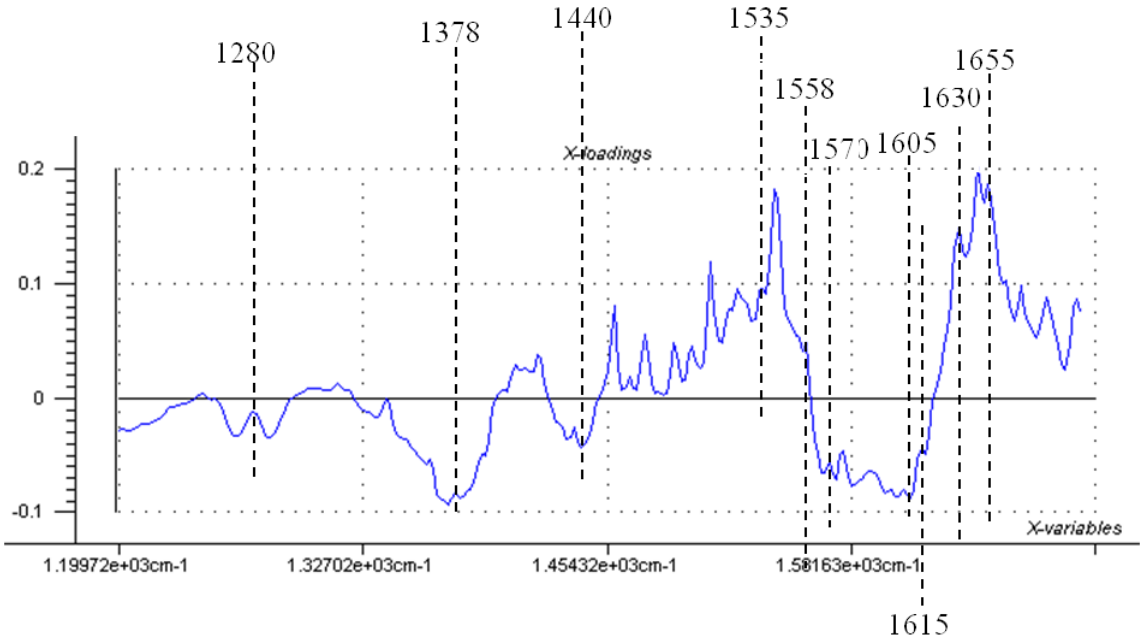
Figure 5-6 shows the spore survival curve with NTP using air or argon as feed gas. Compared with the air feed gas NTP, survival curve of NTP with argon as feed gas was linear indicating the inactivation process was homogeneous. Also, the inactivation rate is

not as high as air NTP because in this process no reactive species would be generated, which might play an important role in spore inactivation.

Figure 5-7A and 5-8A are the score plots of control spores and spores after autoclave and high pressure treatments. These two treatments can be separated from the control by PC2. Figure 5-7B and 5-8B are loading plots of control spores and spores after autoclave and high pressure treatment in PC2. Peaks in loading plots are sharper then original spectra and it helps to analyze the spectra. Figure 5-7B shows that loading values of DPA bands (1280, 1378, 1440, 1570, 1605, 1615 cm^{-1}) were small, which indicates the total amount of DPA after autoclave was close to the control spores, and so did the high pressure treatment as indicated in Figure 5-8B. Loading values of all protein bands (1535, 1558, 1630, 1655 cm^{-1}) in Figure 5-7B were large, indicating that both α-helical structure and β-pleated sheets structure changed after autoclave treatment. Loading values of protein bands of 1535, 1558, 1655 cm^{-1}) in Figure 5-8B were large, however, the loading value of 1630 cm^{-1} was small, indicating that the protein structure changed after high pressure treatment except β-pleated sheets structure. It is reasonable because β-pleated sheet is parallel structure and trend not to be altered by high pressure.

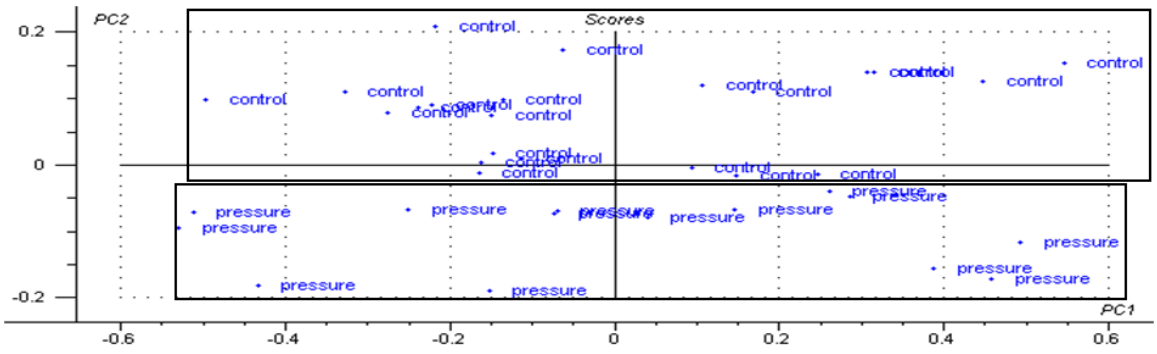


(A) Score plot of control spores and spores after autoclave treatment

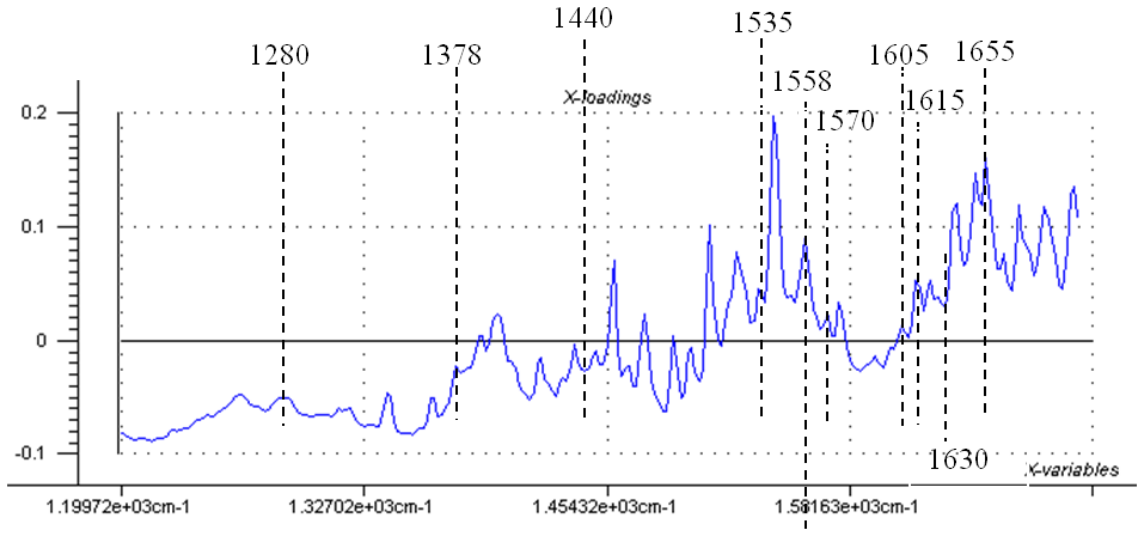


(B) Loading plot of control spores and spores after autoclave treatment in PC2

Figure 5- 7 Principal component analysis of control spores and spores after autoclave treatment



(A) Score plot of control spores and spores after high pressure treatment



(B) Loading plot of control spores and spores after high pressure treatment in PC2

Figure 5- 8 Principal component analysis of control spores and spores after high pressure treatment

5.5 Conclusion

Spores morphology after different treatments was observed by SEM and TEM. SEM and TEM images showed that it was possible that mechanical forces were the essential cause for the spore inactivation by heat and high-pressure, while CD and NTP with air as ffed gas treatments inactivated spores by oxidation reaction; and NTP with argon as feed

gas treatment inactivated spores by UV emission or charged particle. Multivariate pattern recognition based upon FTIR spectra was developed to study the biochemical composition change of the BA spore. The spectra indicates that 1) CD oxidized spores (peptides, DPA, etc.) and generated carboxylate; 2) DPA bands decreased after NTP with air as feed gas treatment; 3) DPA bands increased after NTP with argon as feed gas treatment; 4) DPA bands did not have significant change after autoclave and high pressure treatments; 5) both α-helical structure and β-pleated sheets structure changed after autoclave treatment, while only α-helical structure changed after high pressure treatment. This methodology will provide a useful new tool to rapidly examine bacterial spores after different sporicidal treatments. Further research is needed to confirm conclusions above drew by FTIR spectra. The comparison of air NTP and argon NTP indicated that reactive species played an important role in spore inactivation.

OVERALL SUMMARY AND PERSPECTIVE

Bacterial spores are resistant to adverse conditions, for example, heat, high pressure and extreme pH. Because of its resistance, bacterial spores can cause spoilage which results in large economic losses and has become a primary concern in the food industry. Besides, it is easy for terrorists to make biowarfare using bacterial spores such as anthrax. Non-thermal plasma (NTP) is a newly developing method as an alternative for traditional autoclave and chemical treatments due to its non-thermal and cost-effective features.

In this study, non-thermal plasma (NTP) inactivation of Bacillus Amyloliquefaciens spores was investigated using FTIR as a major tool. Spore morphology and biochemical properties after NTP (if not mentioned, the feed gas is air by default) treatment were studied. The kinetic study showed that the inactivation rate was high first and then began to slow down at about 3 min. The bi-slope survival curve observed in our study likely occurred because NTP inactivation was only a surface treatment, thus resulting reactive species such as ozone and other oxidants were initially unable to penetrate spores in the bottom layers. Cell debris accumulation during the rapid initial inactivation phase leads to a slower secondary inactivation phase. The topography of spore surface showed that plasma might have static force on the multi-layered spores and continued to disintegrate the spore stack such that the reactive species could reach the bottom layers of spores to inactivate them, albeit, at a slower rate. Spore surface was etched away by plasma. During NTP inactivation, DPA released and then reacted with reactive species, while proteins denatured and aggregated.

Spore germination was monitored by FTIR and UV-Vis spectroscopy. The

combination of UV-Vis spectroscopy and ATR-FTIR can provide more information about spore germination by linking fraction of germinated spores to specific molecular changes, especially DPA. The germination of spore in suitable temperatures was fast at first and then slowed down and DPA release was similar to this pattern. DPA release of spores germinated at 50 ℃ increased dramatically at the beginning (about 4 min) indicating unnatural DPA release due to heat, and the fraction of germinated spore was lowest. The DPA release of NTP treated spores was lowest because DPA released and reacted with reactive species generated by NTP. The NTP treated spores could germinate but with a lower fraction compared with ones grew at suitable condition. Also lines of protein bands of NTP treated spores along time wiggled indicating that plasma might induce sub-lethal effect on spores and protein synthesis was disordered. Weibull model was built to describe spore germination but it cannot be applied to NTP treated spores and it showed that NTP treated spores exhibited different germination pattern.

NTP treatments were compared with autoclave, chemical treatment (chlorine dioxide), and high pressure treatments. Besides, air and argon were used as feed gas in NTP treatments and they were compared. FTIR spectra of autoclave, high pressure and NTP with argon as feed gas treated spores had larger absorbance compared with the control. However, spectra of CD treated spores had lower absorbance especially between 1492 cm^{-1} and 1566 cm^{-1} and the shape changed. Also the spectra of NTP with air as feed gas treated spores had the lowest absorbance. The comparison showed that autoclave and high pressure inactivated spores by mechanic force as no changes in DPA bands; while chemical treatment and NTP with air as feed gas treatment inactivated spores by oxidation. Chlorine dioxide might oxidize DPA and carboxylate was generated. DPA was

released during NTP with argon as feed gas treatment, and UV emission or charged particle might account for the inactivation. Compared with the air feed gas NTP, survival curve of NTP with argon as feed gas was linear indicating the inactivation process was homogeneous. Also, the inactivation rate was not as high as air NTP because in this process no reactive species would be generated, which might play an important role in spore inactivation.

In future study, further researches are needed to find out how to apply NTP technique in food industry and for medical uses. Our study can provide some information in optimizing parameters in the process.

LIST OF REFERENCES

1. Vries, Y.P.d., *Bacillus cereus spore formation, structure, and germination*. 2006, Wageningen University,: Wageningen. p. 128.
2. Kuo*, S.P., *Plasma Assisted Decontamination of Bacterial Spores.* Open Biomed Eng J., 2008. **2**: p. 36-42.
3. Rotz, L.D., et al., *Public health assessment of potential biological terrorism agents.* Emerging Infectious Diseases, 2002. **8**(2): p. 225-230.
4. Tepper, M. and J. Whitehead, *Clinical predictors of bioterrorism-related inhalational anthrax.* Lancet, 2005. **365**(9455): p. 214-214.
5. Friedrich, L.M., et al., *Mitigation of Alicyclobacillus spp. spores on food contact surfaces with aqueous chlorine dioxide and hypochlorite.* Food Microbiology, 2009. **26**(8): p. 936-941.
6. Akhtara, S., et al., *Strategy to inactivate Clostridium perfringens spores in meat products.* Food Microbiology, 2009. **26**(3): p. 272-277.
7. Blatchley, E.R., et al., *Inactivation of Bacillus spores by ultraviolet or gamma radiation.* Journal of Environmental Engineering-Asce, 2005. **131**(9): p. 1245-1252.
8. Hall, H.E. and Angelott.R, *Clostridium perfringeds in meat and meat products.* Applied Microbiology, 1965. **13**(3): p. 352-&.
9. Moreau, M., N. Orange, and M.G.J. Feuilloley, *Non-thermal plasma technologies: New tools for bio-decontamination.* Biotechnology Advances, 2008. **26**(6): p. 610-617.
10. Moisan, M., et al., *Low-temperature sterilization using gas plasmas: a review of the experiments and an analysis of the inactivation mechanisms.* International Journal of Pharmaceutics, 2001. **226**(1-2): p. 1-21.
11. Shulzinger, A., A. Abramovich, and E. Farber. *Attenuated Total Reflectance (ATR)-FTIR spectral measurements in MIR and FIR (THz) range*. in *Microwaves, Communications, Antennas and Electronics Systems, 2009. COMCAS 2009. IEEE International Conference on*. 2009.
12. Subramanian, A., et al., *Determination of spore inactivation during thermal and pressure-assisted thermal processing using FT-IR spectroscopy.* Journal of Agricultural and Food Chemistry, 2006. **54**(26): p. 10300-10306.
13. Subramanian, A., et al., *Monitoring biochemical changes in bacterial spore during thermal and pressure-assisted thermal processing using FT-IR Spectroscopy.* Journal of Agricultural and Food Chemistry, 2007. **55**(22): p. 9311-9317.
14. Driks, A., *Bacillus subtilis spore coat.* Microbiology and Molecular Biology Reviews, 1999. **63**(1): p. 1-+.
15. Gerhardt, P. and E. Ribi, *Ultrastructure of exosporium enveloping spores of Bacillus cereus.* Journal of Bacteriology, 1964. **88**(6): p. 1774-&.
16. Riesenman, P.J. and W.L. Nicholson, *Role of the spore coat layers in Bacillus subtilis spore resistance to hydrogen peroxide, artificial UV-C, UV-B, and solar UV radiation.* Applied and Environmental Microbiology, 2000. **66**(2): p. 620-626.
17. Nicholson, W.L., et al., *Resistance of Bacillus endospores to extreme terrestrial and extraterrestrial environments.* Microbiology and Molecular Biology Reviews, 2000. **64**(3): p. 548-+.

18. Paidhungat, M., et al., *Characterization of spores of Bacillus subtilis which lack dipicolinic acid.* Journal of Bacteriology, 2000. **182**(19): p. 5505-5512.
19. Setlow, P., *Mechanisms for the prevention of damage to DNA in spores of Bacillus species.* Annual Review of Microbiology, 1995. **49**: p. 29-54.
20. Popham, D.L., *Specialized peptidoglycan of the bacterial endospore: the inner wall of the lockbox.* Cellular and Molecular Life Sciences, 2002. **59**(3): p. 426-433.
21. Atrih, A. and S.J. Foster, *Bacterial endospores the ultimate survivors.* International Dairy Journal, 2002. **12**(2-3): p. 217-223.
22. Bagyan, I. and P. Setlow, *Localization of the cortex lytic enzyme CwlJ in spores of Bacillus subtilis.* Journal of Bacteriology, 2002. **184**(4): p. 1219-1224.
23. Moir, A., B.M. Corfe, and J. Behravan, *Spore germination.* Cellular and Molecular Life Sciences, 2002. **59**(3): p. 403-409.
24. Park, T.J., et al., *Spore Display Using Bacillus thuringiensis Exosporium Protein InhA.* Journal of Microbiology and Biotechnology, 2009. **19**(5): p. 495-501.
25. Mader, S., *Biology*. 9 ed. 2007.
26. Errington, J., *Regulation of endospore formation in Bacillus subtilis.* Nature Reviews Microbiology, 2003. **1**(2): p. 117-126.
27. Weaver, R.F., *Molecular Biology*. 4 ed.
28. Kay, D. and S.C. Warren, *Sporulation in Bacillus subtilis morphological changes.* Biochemical Journal, 1968. **109**(5): p. 819-&.
29. Russell, A.D., *Bacterial-spores and chemical sporicidal agents.* Clinical Microbiology Reviews, 1990. **3**(2): p. 99-119.
30. Hashimot.T and S.F. Conti, *Ultrastructural changes associated with activation and germination of Bacillus cereus spores.* Journal of Bacteriology, 1971. **105**(1): p. 361-&.
31. Hudson, K.D., et al., *Localization of GerAA and GerAC germination proteins in the Bacillus subtilis spore.* Journal of Bacteriology, 2001. **183**(14): p. 4317-4322.
32. Setlow, P., *Spore germination.* Current Opinion in Microbiology, 2003. **6**(6): p. 550-556.
33. Craggs, J.M.M.a.J.D., *Electrical Breakdown of gases*. 1978, Hoboken, NJ: Wiley.
34. H.Raether, *Electron Avalanches and Breakdown in Gasses*. 1964, London, U.K.: Butterworth.
35. Kogelschatz, U., *Dielectric-barrier discharges: Their history, discharge physics, and industrial applications.* Plasma Chemistry and Plasma Processing, 2003. **23**(1): p. 1-46.
36. Egli, W. and U. Kogelschatz, *Space-charge formation around a high-voltage corona electrode in electrostatic precipitators.* Helvetica Physica Acta, 1995. **68**(2): p. 203-204.
37. Conrads, H. and M. Schmidt, *Plasma generation and plasma sources.* Plasma Sources Science & Technology, 2000. **9**(4): p. 441-454.
38. Kogelschatz, U., *Filamentary, patterned, and diffuse barrier discharges.* Ieee Transactions on Plasma Science, 2002. **30**(4): p. 1400-1408.

39. Kraus, M., et al., *CO_2 reforming of methane by the combination of dielectric-barrier discharges and catalysis.* Physical Chemistry Chemical Physics, 2001. **3**(3): p. 294-300.
40. Laroussi, M., *Low temperature plasma-based sterilization: Overview and state-of-the-art.* Plasma Processes and Polymers, 2005. **2**(5): p. 391-400.
41. Herrmann, H.W., et al., *Decontamination of chemical and biological warfare, (CBW) agents using an atmospheric pressure plasma jet (APPJ).* Physics of Plasmas, 1999. **6**(5): p. 2284-2289.
42. Laroussi, M., et al., *Images of biological samples undergoing sterilization by a glow discharge at atmospheric pressure.* Ieee Transactions on Plasma Science, 1999. **27**(1): p. 34-35.
43. Yamamoto, M., M. Nishioka, and M. Sadakata, *Sterilization by H2O2 droplets under corona discharge.* Journal of Electrostatics, 2002. **55**(2): p. 173-187.
44. Boudam, M.K., et al., *Bacterial spore inactivation by atmospheric-pressure plasmas in the presence or absence of UV photons as obtained with the same gas mixture.* Journal of Physics D-Applied Physics, 2006. **39**(16): p. 3494-3507.
45. Kelly-Wintenberg, K., et al., *Room temperature sterilization of surfaces and fabrics with a One Atmosphere Uniform Glow Discharge Plasma.* Journal of Industrial Microbiology & Biotechnology, 1998. **20**(1): p. 69-74.
46. Laroussi, M., I. Alexeff, and W.L. Kang, *Biological decontamination by nonthermal plasmas.* Ieee Transactions on Plasma Science, 2000. **28**(1): p. 184-188.
47. Kelly-Wintenberg, K., et al., *Use of a one atmosphere uniform glow discharge plasma to kill a broad spectrum of microorganisms.* Journal of Vacuum Science & Technology a-Vacuum Surfaces and Films, 1999. **17**(4): p. 1539-1544.
48. Roth, J.R., et al., *A remote exposure reactor (RER) for plasma processing and sterilization by plasma active species at one atmosphere.* Ieee Transactions on Plasma Science, 2000. **28**(1): p. 56-63.
49. Feng, H.Q., et al., *The Interaction of a Direct-Current Cold Atmospheric-Pressure Air Plasma With Bacteria.* Ieee Transactions on Plasma Science, 2009. **37**(1): p. 121-127.
50. Laroussi, M., *Sterilization of contaminated matter with an atmospheric pressure plasma.* Ieee Transactions on Plasma Science, 1996. **24**(3): p. 1188-1191.
51. Laroussi, M., *Nonthermal decontamination of biological media by atmospheric-pressure plasmas: Review, analysis, and prospects.* Ieee Transactions on Plasma Science, 2002. **30**(4): p. 1409-1415.
52. Norman, A., *The nuclear role in the ultraviolet inactivation of Neurospora conidia.* Journal of Cellular and Comparative Physiology, 1954. **44**(1): p. 1-10.
53. Gaunt, L.F., C.B. Beggs, and G.E. Georghiou, *Bactericidal action of the reactive species produced by gas-discharge nonthermal plasma at atmospheric pressure: A review.* Ieee Transactions on Plasma Science, 2006. **34**(4): p. 1257-1269.
54. Harm, W., *Biological Effects of Ultravialet Radiation*. Vol. ch.3. 1980, Cambridge, U.K.: Cambridge Univ. Press.
55. Jagger, J., *Introduction to Research in Ultraviolet Photobiology*. Vol. ch. 4. 1967, Englewood Clliffs, NJ: Prentice-Hall.

56. Laroussi, M. and F. Leipold, *Evaluation of the roles of reactive species, heat, and UV radiation in the inactivation of bacterial cells by air plasmas at atmospheric pressure.* International Journal of Mass Spectrometry, 2004. **233**(1-3): p. 81-86.
57. Schutze, A., et al., *The atmospheric-pressure plasma jet: A review and comparison to other plasma sources.* Ieee Transactions on Plasma Science, 1998. **26**(6): p. 1685-1694.
58. Shibata, M., N. Nakano, and T. Makabe, *Effect of O-2(a(1)Delta(g)) on plasma structures in oxygen radio frequency discharges.* Journal of Applied Physics, 1996. **80**(11): p. 6142-6147.
59. E. Cabiscol, J.T., and J. Ros, *Oxidative stress in bacteria and protein damage by reactive oxygen species.* International Microbioly, 2000. **3**(1): p. 3-8.
60. Farr, S.B. and T. Kogoma, *Oxidative stress responses in Escherichia coli and Salmonella typhimurium.* Microbiological Reviews, 1991. **55**(4): p. 561-585.
61. Humphries, K.M. and L.I. Szweda, *Selective inactivation of alpha-ketoglutarate dehydrogenase and pyruvate dehydrogenase: Reaction of lipoic acid with 4-hydroxy-2-nonenal.* Biochemistry, 1998. **37**(45): p. 15835-15841.
62. Singh, A. and H. Singh, *Time-scale and nature of radiation biological damage approaches to radiation protection and post-irradiation therapy.* Progress in Biophysics & Molecular Biology, 1982. **39**(2): p. 69-107.
63. Berlett, B.S. and E.R. Stadtman, *Protein oxidation in aging, disease, and oxidative stress.* Journal of Biological Chemistry, 1997. **272**(33): p. 20313-20316.
64. Stadtman, E.R., *Protein oxidation and aging.* Science, 1992. **257**(5074): p. 1220-1224.
65. Dean, R.T., et al., *Biochemistry and pathology of radical-mediated protein oxidation.* Biochemical Journal, 1997. **324**: p. 1-18.
66. Grune, T., T. Reinheckel, and K.J.A. Davies, *Degradation of oxidized proteins in mammalian cells.* Faseb Journal, 1997. **11**(7): p. 526-534.
67. Segerback, D., *Alkylation of DNA and hemoglobin in the mouse following exposure to ethene and ethene oxide.* Chemico-Biological Interactions, 1983. **45**(2): p. 139-151.
68. Summerfield, F.W. and A.L. Tappel, *Determination by fluorescence quenching of the environment of DNA crosslinks made by malondialdehyde.* Biochimica Et Biophysica Acta, 1983. **740**(2): p. 185-189.
69. Mendis, D.A., M. Rosenberg, and F. Azam, *A note on the possible electrostatic disruption of bacteria.* Ieee Transactions on Plasma Science, 2000. **28**(4): p. 1304-1306.
70. Laroussi, M., D.A. Mendis, and M. Rosenberg, *Plasma interaction with microbes.* New Journal of Physics, 2003. **5**.
71. Sun, Y.Z., et al., *Experimental research on inactivation of bacteria by using dielectric barrier discharge.* Ieee Transactions on Plasma Science, 2007. **35**(5): p. 1496-1500.
72. Lu, X., et al., *The roles of the various plasma agents in the inactivation of bacteria.* Journal of Applied Physics, 2008. **104**(5).

73. Shi, X.M., et al., *Research on the inactivation effect of low-temperature plasma on Candida albicans.* Ieee Transactions on Plasma Science, 2008. **36**(2): p. 498-503.
74. Fridman, G., et al., *Comparison of direct and indirect effects of non-thermal atmospheric-pressure plasma on bacteria.* Plasma Processes and Polymers, 2007. **4**(4): p. 370-375.
75. Deng, X.T., J.J. Shi, and M.G. Kong, *Physical mechanisms of inactivation of Bacillus subtilis spores using cold atmospheric plasmas.* Ieee Transactions on Plasma Science, 2006. **34**(4): p. 1310-1316.
76. Kim, S.J., et al., *Bacterial inactivation using atmospheric pressure single pin electrode microplasma jet with a ground ring.* Applied Physics Letters, 2009. **94**(14).
77. Park, B.J., et al., *Sterilization using a microwave-induced argon plasma system at atmospheric pressure.* Physics of Plasmas, 2003. **10**(11): p. 4539-4544.
78. Laroussi, M., J.P. Richardson, and F.C. Dobbs, *Effects of nonequilibrium atmospheric pressure plasmas on the heterotrophic pathways of bacteria and on their cell morphology.* Applied Physics Letters, 2002. **81**(4): p. 772-774.
79. Perkins, D.L., et al., *Effects of autoclaving on bacterial endospores studied by Fourier transform infrared microspectroscopy.* Applied Spectroscopy, 2004. **58**(6): p. 749-753.
80. Helm, D. and D. Naumann, *Identification of some bacterial-cell components by FT-IR spectroscopy.* Fems Microbiology Letters, 1995. **126**(1): p. 75-79.
81. Cheung, H.Y., J.X. Cui, and S.Q. Sun, *Real-time monitoring of Bacillus subtilis endospore components by attenuated total reflection Fourier-transform infrared spectroscopy during germination.* Microbiology-Sgm, 1999. **145**: p. 1043-1048.
82. Margosch, D., et al., *High-pressure-mediated survival of Clostridium botulinum and Bacillus amyloliquefaciens endospores at high temperature.* Applied and Environmental Microbiology, 2006. **72**(5): p. 3476-3481.
83. Feeherry, F., D.T. Munsey, and D.B. Rowley, *Thermal inactivation and injury of Bacillus stearothermophilus spores.* Applied and Environmental Microbiology, 1987. **53**(2): p. 365-370.
84. Loshon, C.A., et al., *Levels of glycine betaine in growing cells and spores of Bacillus species and lack of effect of glycine betaine on dormant spore resistance.* Journal of Bacteriology, 2006. **188**(8): p. 3153-3158.
85. Naumann, D., D. Helm, and H. Labischinski, *Microbiological characterizations by FTIR spectroscopy.* Nature, 1991. **351**(6321): p. 81-82.
86. Yu, C.X., et al., *Spectroscopic differentiation and quantification of microorganisms in apple juice.* Journal of Food Science, 2004. **69**(7): p. S268-S272.
87. Beekes, M., P. Lasch, and D. Naumann, *Analytical applications of Fourier transform-infrared (FT-IR) spectroscopy in microbiology and prion research.* Veterinary Microbiology, 2007. **123**(4): p. 305-319.
88. Perkins, D.L., et al., *Fourier transform infrared reflectance microspectroscopy study of Bacillus subtilis engineered without dipicolinic acid: The contribution of*

calcium dipicolinate to the mid-infrared absorbance of Bacillus subtilis endospores. Applied Spectroscopy, 2005. **59**(7): p. 893-896.
89. Goodacre, R., et al., *Detection of the dipicolinic acid biomarker in Bacillus spores using Curie-point pyrolysis mass spectrometry and fourier transform infrared spectroscopy.* Analytical Chemistry, 2000. **72**(1): p. 119-127.
90. Jian Li, S.L., Shujun Li, Jing Wang and Dan Liu, *Synthesis of A Rosin Amide and Its Inhibition of Wood Decay Fungi.* Advanced Materials Research, 2010. **113-116**: p. 2232-2236.
91. Yu, C.X. and J. Irudayaraj, *Spectroscopic characterization of microorganisms by Fourier transform infrared microspectroscopy.* Biopolymers, 2005. **77**(6): p. 368-377.
92. Tremmel, S., et al., *C-13-labeled tyrosine residues as local IR probes for monitoring conformational changes in peptides and proteins.* Angewandte Chemie-International Edition, 2005. **44**(29): p. 4631-4635.
93. Setlow, B., et al., *Role of dipicolinic acid in resistance and stability of spores of Bacillus subtilis with or without DNA-protective alpha/beta-type small acid-soluble proteins.* Journal of Bacteriology, 2006. **188**(11): p. 3740-3747.
94. Setlow, P., *Spores of Bacillus subtilis: their resistance to and killing by radiation, heat and chemicals.* Journal of Applied Microbiology, 2006. **101**(3): p. 514-525.
95. Kong, L.B., et al., *Characterization of Bacterial Spore Germination Using Integrated Phase Contrast Microscopy, Raman Spectroscopy, and Optical Tweezers.* Analytical Chemistry, 2010. **82**(9): p. 3840-3847.
96. Plowman, J. and M.W. Peck, *Use of a novel method to characterize the response of spores of non-proteolytic Clostridium botulinum types B, E and F to a wide range of germinants and conditions.* Journal of Applied Microbiology, 2002. **92**(4): p. 681-694.
97. Paredes-Sabja, D., et al., *Characterization of Clostridium perfringens spores that lack spoVA proteins and dipicolinic acid.* Journal of Bacteriology, 2008. **190**(13): p. 4648-4659.
98. Paredes-Sabja, D., et al., *Clostridium perfringens spore germination: Characterization of germinants and their receptors.* Journal of Bacteriology, 2008. **190**(4): p. 1190-1201.
99. Collado, J., et al., *Modelling the effect of a heat shock and germinant concentration on spore germination of a wild strain of Bacillus cereus.* International Journal of Food Microbiology, 2006. **106**(1): p. 85-89.
100. Paredes-Sabja, D. and J.A. Torres, *Modeling of the germination of spores from Clostridium perfringens food poisoning isolates.* Journal of Food Process Engineering, 2010. **33**: p. 150-167.
101. Fernandez, A., et al., *Empirical model building based on Weibull distribution to describe the joint effect of pH and temperature on the thermal resistance of Bacillus cereus in vegetable substrate.* International Journal of Food Microbiology, 2002. **77**(1-2): p. 147-153.
102. Mafart, P., et al., *On calculating sterility in thermal preservation methods: application of the Weibull frequency distribution model.* International Journal of Food Microbiology, 2002. **72**(1-2): p. 107-113.

103. Ross, T., *Indices for performance evaluation of predictive models in food microbiology.* Journal of Applied Bacteriology, 1996. **81**(5): p. 501-508.
104. Baranyi, J., C. Pin, and T. Ross, *Validating and comparing predictive models.* International Journal of Food Microbiology, 1999. **48**(3): p. 159-166.
105. Lebert, I., V. Robles-Olvera, and A. Lebert, *Application of polynomial models to predict growth of mixed cultures of Pseudomonas spp. and Listeria in meat.* International Journal of Food Microbiology, 2000. **61**(1): p. 27-39.
106. Esbensen, K., *Multivariate Analysis - in practice*. 3rd ed. 1998: CAMO.

VITA

Yaohua Huang was born in Shenzhen, Guangdong, China. He grew up in his hometown and was admitted by Sun Yat-sen University in 2004. He went to Guangzhou and finished his Bachelor of Science degree, double major in Biotechnology and Chemistry. After graduation in 2008, he worked in Shenzhen Academic of Metrology and Quality Inspection as quality assurance engineer and began preparing for the application of overseas study. In the summer of 2009, he went to the United States and pursued a Master of Science degree in Biosystems Engineering at the University of Tennessee, Knoxville. Two years later in 2011, he completed a Master's degree in Biosystems Engineering and minor in Statistics.